

Circuit model of ballistic multiterminal Josephson junctions

Régis Mélin¹

¹Univ. Grenoble-Alpes, CNRS, Grenoble INP, Institut NEEL, 38000 Grenoble, France

Nonequilibrium multiterminal superconducting devices have focused considerable interest recently in connection with Floquet theory and/or nontrivial topology. Here, we consider ballistic multiterminal Josephson junctions having length scales intermediate between the short- and long-junction limits, taking the example of four terminals. We propose a phenomenological circuit model for the quartets, that relies on nonlocal ballistic Andreev resonances within the superconducting gap, and on relaxation in the nonproximitized regions of the ballistic metal. The interplay between nonlocal two-Cooper pair resonances and relaxation produces anomalously large quartet current at low-bias voltage within a two-node model. Gating away from particle-hole symmetry favors “absence of inversion” followed by “inversion” as the bias voltage increases, where “inversion” refers to the counterintuitive larger critical current at half flux-quantum than in zero field. The model is qualitatively compatible with the recent Harvard group experiment on graphene-based four-terminal Josephson junctions.

I. INTRODUCTION

BCS superconductors [1] are characterized by macroscopic phase variable φ and energy gap Δ between the ground state and the first quasiparticles. The Cooper pairs are nonentangled as long as they stay in the bulk of a BCS condensate. In superconductor-normal metal (SN) structures, the direct BCS attractive interaction is solely operational in the superconductor S , but the Cooper pairs from S can be transmitted as Andreev pairs into the normal part N of the junction, keeping their two-electron superconducting coherence at long distance from the interface. Those entangled Andreev pairs can split if two independent voltages are applied in three-terminal F_aSF_b ferromagnet-superconductor-ferromagnet or N_aSN_b normal metal-superconductor-normal metal Cooper pair beam splitters [2–29]. “Nonlocal Andreev reflection” or, said differently, “crossed Andreev reflection” (CAR) appears if the separation between the N_aS and SN_b interfaces is comparable to the zero-energy superconducting coherence length. Spin-up electron from lead N_b can be Andreev reflected as spin-down hole into N_a , leaving a Cooper pair in the “central” S . As a result of those nonlocally split Cooper pairs, the current I_a through N_a is sensitive to the bias voltage V_b on N_b [2–29]. In addition, the positive current-current cross-correlations of Cooper pair splitting [4, 30–41] were experimentally revealed [23, 24].

Regarding those normal metal-superconductor-normal metal Cooper pair beam splitters [16–29], the double quantum dot experiments [21, 22, 24] provide evidence for non-local two-particle Andreev resonance in N_a -dot- S_c -dot- N_b devices, on the condition of opposite energy levels $\epsilon_a = -\epsilon_b$ on both quantum dots. In the following, we demonstrate how “nonlocal two-particle Andreev resonance” in N_a -dot- S_c -dot- N_b Cooper pair beam splitters can be generalized to “nonlocal two-Cooper pair resonance” in all-superconducting three-terminal S_a - S_c - S_b Josephson junctions.

Those two-Cooper pair resonances build on nonlocal two-Cooper pair states, the so-called quartets [42–55] that appear in (S_a, S_c, S_b) three-terminal Josephson junctions, where S_a and S_b are voltage-biased at V_a and V_b , and S_c is grounded at $V_c = 0$. Andreev scattering yields quartet phase-sensitive DC-current response if the condition $V_a = -V_b \equiv V$ is fulfilled. On

this quartet line $V_a = -V_b$, the elementary transport process transfers two Cooper pairs from S_a and S_b into the grounded S_c , while exchanging partners [42–55]. By the time-energy uncertainty relation, this phase-sensitive quartet current is DC, since, on the quartet line, the energy $E_i = 2e(V_a + V_b)$ of two Cooper pairs from S_a and S_b in the initial state is equal to $E_f = 4eV_c$ for two Cooper pairs transmitted into S_c in the final state.

Several experiments were recently performed on multiterminal Josephson junctions [56–65]. Some of those explored the possibility of nontrivial topology [55, 57, 66–82]. On the other hand, three groups reported compatibility with the quartets [42–55]: the Grenoble group experiment with metallic structures [56], the Weizmann Institute group experiment with semiconducting nanowires [58] and the more recent Harvard group experiment on ballistic graphene-based four-terminal Josephson junctions [60]. This third experiment [60] produces characteristic variations for the value of the quartet current as a function of the bias voltage V and the magnetic flux Φ through the loop, and reports the counterintuitive voltage- V -tunable inversion, i.e. stronger quartet current at half-flux quantum $\Phi = \pi$ than in zero field $\Phi = 0$.

A challenge for the theory is to model devices that are quite complex, with e.g. extended interfaces, four or more superconducting leads, nonequilibrium voltage biasing conditions, loops connecting superconducting terminals, possibly with radio-frequency radiation. Direct diagonalizations of the Bogoliubov-de Gennes Hamiltonian would apparently lead to prohibitive computational expenses. We logically develop approximation schemes that allow capturing the effect on the experimental signal of various assumptions about the device. For instance, a useful approximation is to propose simple circuits containing a few nodes, as in finite-element theory. In the field of mesoscopic superconductivity, Nazarov and co-workers (see Ref. 83 and references therein) proposed and developed the superconducting-normal metal circuit theory that describes the proximity effect, i.e. the interplay between Andreev reflection and multiple scattering on disorder. This dirty-limit circuit theory was proposed for multiterminal Josephson junctions [67, 84]. However, the dirty limit implies short elastic mean free path, a condition that is not directly met in the ballistic metals that are currently used in

some experiments on superconducting hybrid structures, such as carbon nanotubes [85], semiconducting nanowires [65] or graphene [86–88]. Specifically, tunneling spectroscopy of carbon nanotube Josephson junctions [85] revealed discrete Andreev bound states. Andreev molecules were realized with semiconducting nanowires [65]. Evidence for superconducting phase difference-sensitive continuum of Andreev bound states was obtained in superconductor-graphene-superconductor Josephson junctions [86, 87]. Microwave experiments on short superconductor-graphene-superconductor Josephson junctions were recently carried out, and modeled with single-level quantum dots [88].

Compared to the single-quantum dot for graphene-superconductor hybrids in the short-junction limit, see the above mentioned Ref. [88], we consider here ballistic multiterminal Josephson junctions that are somewhat larger, and intermediate between the short- and long-junction limits, thus with a few Andreev bound states within the superconducting gap. Then, we naturally model those devices with double quantum dots or larger finite-size tight-binding lattices connected to superconducting leads. In addition, the junction is coupled to normal reservoirs in order to capture the electronic continua in the nonproximitized regions of the ballistic electron gas on which the superconducting leads are evaporated. Thus, the model includes two central physical ingredients: the nonlocal Andreev resonances typical of ballistic devices, and relaxation. We find that small relaxation has the counterintuitive effect of producing strong enhancement of the quartet current. Compared to our previous Ref. 46, we justify here implementation of a two-node circuit model, instead of the single-node Dynes parameter [89–92] model of Ref. 46. We also include four superconducting leads, instead of three in our previous Ref. 46, which allows discussing the recent four-terminal Harvard group experiment within our approach [60].

In the paper, we base the discussion on four models relying on various assumptions. First, the models A and B [93] refer to lowest-order perturbation theory in the tunnel amplitudes between a ballistic metal and four superconducting leads. Model A (see figures 1d and 1e) corresponds to our previous paper I [50] where a two-dimensional (2D) metal is connected to four superconducting leads. Model B (see figure 1f) corresponds to tunnel coupling between the four superconducting leads and a ballistic 2D or three-dimensional (3D) metal in the short-junction limit. Those models A and B are mostly treated in the Supplemental Material [93] and in section VI of the main text. The remaining of the paper deals with models C and D on figure 2. The comparison between those equivalent models C and D and our previous paper II [51] is the following: Our preceding paper II [51] treated a single quantum dot with relaxation solely originating from the continua of BCS quasiparticles. Relaxation then produces finite line-width broadening δ for the Floquet resonances, which behaves like $\log \delta \sim -\Delta/eV$ at low bias voltage energy eV compared to the superconducting gap Δ [46, 47, 51, 77]. In the four-terminal device of paper II [51], Landau-Zener quantum tunneling reduces the quartet current by coherent superpositions in the dynamics of the two opposite current-carrying Andreev bound states, at voltage values that are close

to avoided crossings in the Floquet spectra. By contrast, in the present work, the interplay between the time-periodic dynamics and relaxation produces sharp resonance peaks in the voltage-dependence of the quartet current, instead of the dips found in our previous paper II [51]. Thus, going from the quantum-coherent single 0D quantum dot Dynes model of Refs. 46, 47, 51, and 77 to the more incoherent relaxation in double quantum dots drastically changes the variations of the quartet current as a function of the bias voltage V .

The paper is organized as follows. The nonlocal two-Cooper pair resonance is introduced in section II. The Hamiltonians are presented in section III. Sections IV and V present our analytical and numerical results respectively. Further discussion of the results is presented in section VI. Concluding remarks are presented in the final section VII.

II. NONLOCAL TWO-COOPER PAIR RESONANCE

In this section, we discuss nonlocal resonances in N_a -dot- S_c -dot- N_b Cooper pair beam splitters and in S_a -dot- S_c -dot- S_b three-terminal Josephson junctions, concluding with four-terminal Josephson junctions.

Figures 3a, 3b and 3c show the condition for nonlocal resonance of elastic cotunneling (EC) [2–15] in N_a -dot- S_c -dot- N_b Cooper pair beam splitters. EC transfers single-particle states from N_a to N_b across S_c , and contributes to negative nonlocal conductance $\mathcal{G}_{a,b} = \partial I_a / \partial V_b$ on the voltage biasing condition $V_a = -V_b$, where I_a is the current transmitted into the normal lead N_a . EC is resonant if both quantum dots D_x and D_y have levels at the same energy $\varepsilon_x = \varepsilon_y$, where $\omega = \varepsilon_x = \varepsilon_y$ is the energy of the incoming electron on figure 3a.

Figures 3d, 3e, 3f show CAR [2–15] in N_a -dot- S_c -dot- N_b Cooper pair beam splitters, which reflects by nonlocal Andreev reflection spin-up electron impinging from N_a as spin-down hole transmitted into N_b , leaving a Cooper pair in the central S_c . CAR contributes for positive value to the nonlocal conductance $\mathcal{G}_{a,b}$ at the bias voltages $V_a = V_b$ and $V_c = 0$. The nonlocal CAR resonance is obtained if the quantum dots D_x and D_y have levels at the opposite energies $\varepsilon_x = -\varepsilon_y \equiv \omega$.

Considering S_a -dot- S_c -dot- S_b three-terminal Josephson junctions, figures 3g, 3h, 3i feature double elastic cotunneling (dEC) [5, 7, 10], which transfers Cooper pairs from S_a to S_b across S_c at the bias voltages $V_a = V_b$. This process is resonant if $\omega = E_0$ (for the spin-up electron crossing D_x or D_y) and $-\omega + 2eV = -E_1$ (for the spin-down hole crossing D_x or D_y). Thus, dEC is resonant if $eV = (E_0 - E_1)/2$ and $\omega = E_0$.

Concerning double crossed Andreev reflection (dCAR) in S_a -dot- S_c -dot- S_b three-terminal Josephson junctions on figures 3j, 3k and 3l, two Cooper pairs from S_a and S_b biased at the voltages $\pm V$ cooperatively enter the grounded S_c , producing transient correlations among four fermions, i.e. the so-called quartets. Then,

$$\omega = E_0 \quad (1)$$

$$-\omega + 2eV = -E_1 \quad (2)$$

are obtained at resonance. Conversely, the same Eqs. (1)-(2)

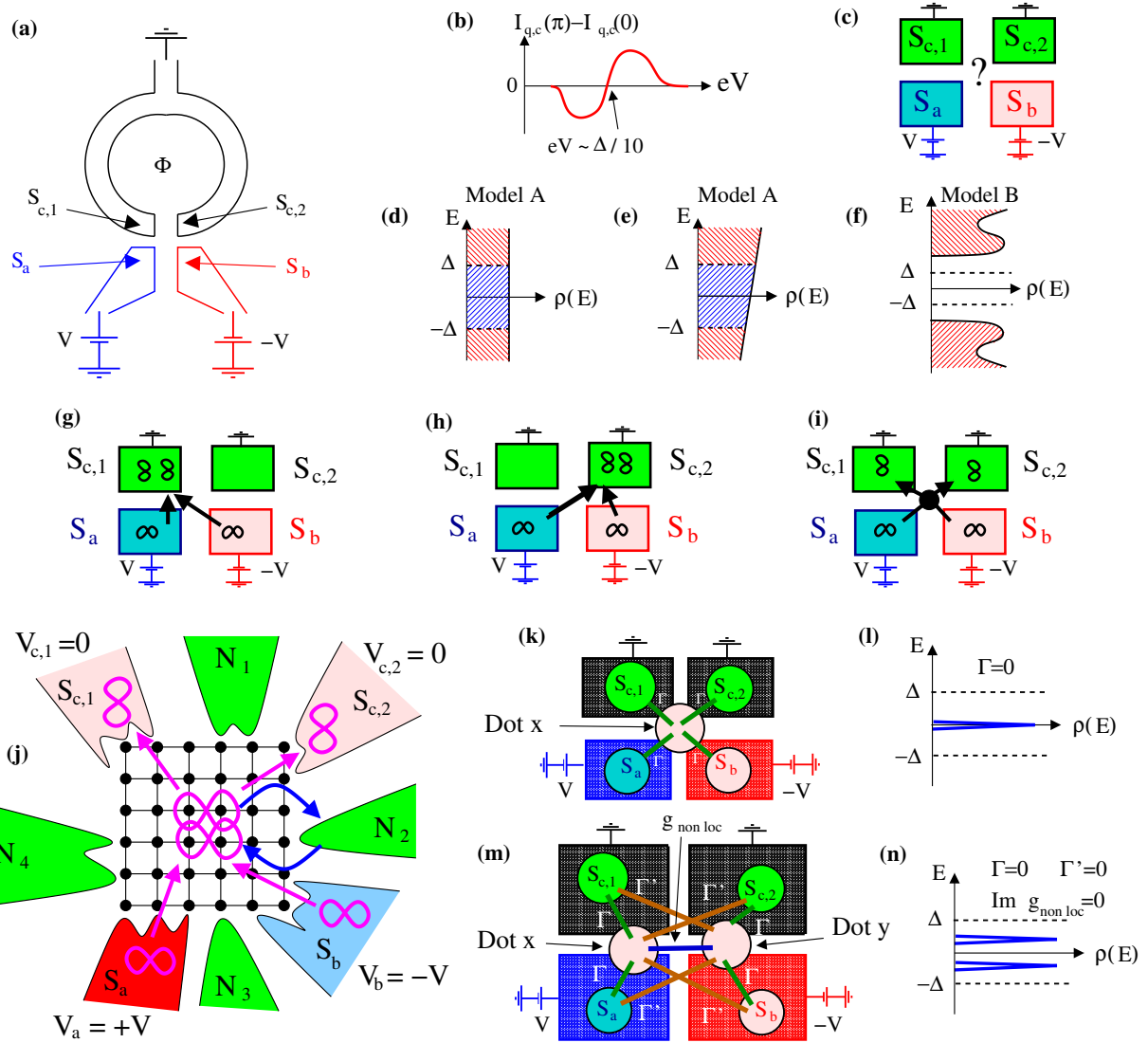


FIG. 1. *The circuit model.* Panel a shows top-view of the Harvard group device [60], corresponding to the four superconducting leads S_a , S_b , $S_{c,1}$ and $S_{c,2}$ evaporated on a sheet of graphene. Panel b sketches the experimental voltage-dependence of $I_{q,c}(\Phi = \pi, eV/\Delta) - I_{q,c}(\Phi = 0, eV/\Delta)$, where the quartet critical current is denoted by $I_{q,c}$. Panel c illustrates that theory should proceed with assumptions about the region making the junction. Panels d-e illustrate the energy-dependence of the density of states (DOS) of the ballistic metal, and panel e shows the DOS of a finite-size two- or three-dimensional metal that is used to model the short-junction limit. Panels g and h represent the Q_1 and Q_2 quartets, and panel i shows the SQ split quartets. The tight-binding model is shown on panel j, with four additionally attached normal leads. Panels k and m show phenomenological single node and two-node circuit models, and the corresponding DOS is shown on panels l and n.

are obtained for resonance of the spin-up electron and spin-down holes crossing D_y .

Coming back to the ballistic multiterminal Josephson junction on figure 1j, we now assume that D_x and D_y are gathered into a single multilevel quantum dot. Assuming the opposite energies $E_0 = -E_1 \equiv \Omega$ implies $\omega = \Omega$ and $-\omega + 2eV = \Omega$, which yields

$$eV = \omega = \Omega \quad (3)$$

for the nonlocal quartet resonance. This Eq. (3) will further be discussed in subsection IV C.

Overall, the argument leading to Eq. (3) suggests that non-local quartet resonance is produced at voltage energy eV that

can be much smaller than the superconducting gap Δ , if the energy scales $\pm\Omega$ are also within $\pm\Delta$. Thus, the small energy scale Ω is built-in for this model of two-Cooper pair resonance.

III. HAMILTONIANS

Now, we provide the Hamiltonians.

We specialize our calculations to the device on figure 1 with four superconducting leads, but the model can be generalized to include larger number of superconducting leads in future calculations.

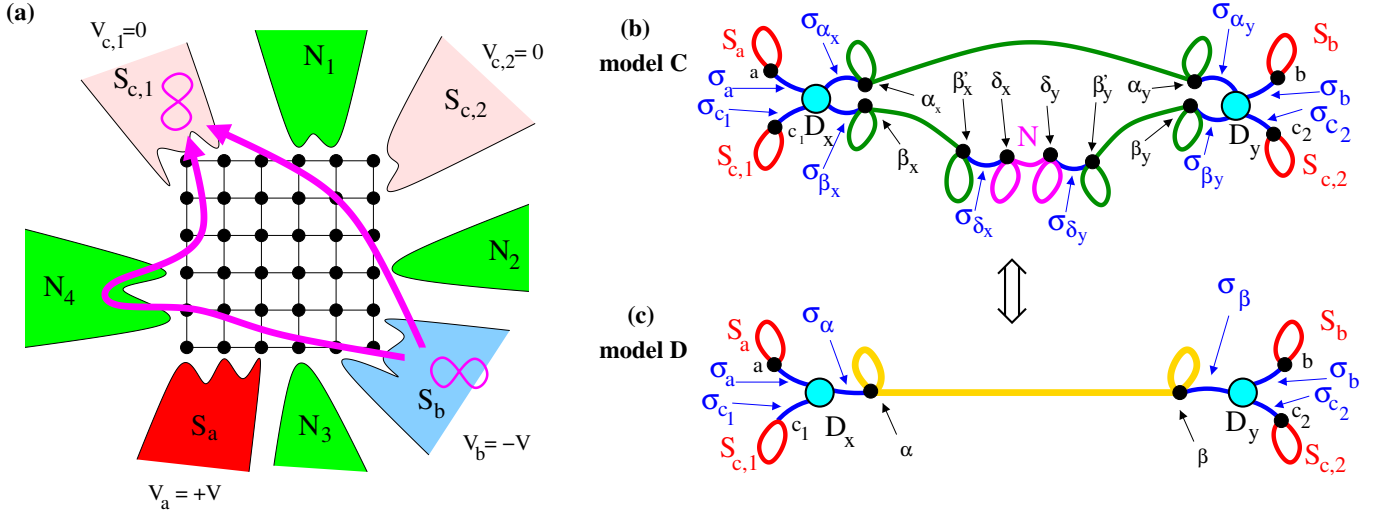


FIG. 2. *The interfering tunneling paths.* Panel a shows interference between the “direct” $S_b \rightarrow \text{dot} \rightarrow S_{c,1}$ tunneling path, and the indirect one $S_b \rightarrow \text{dot} \rightarrow N_4 \rightarrow \text{dot} \rightarrow S_{c,1}$. Panel b features a simple circuit for the interference, between the upper direct and the lower indirect tunneling paths. Panel c shows an equivalent circuit, with the complex-valued Green’s functions given by Eqs. (51)–(54). On this figure, the coupling Γ couples the quantum dot D_x to $(S_a, S_{c,1})$ and D_y to $(S_b, S_{c,2})$. We assume $\Gamma' = 0$, i.e. the quantum dot D_x is not directly coupled to $(S_b, S_{c,2})$, and D_y is uncoupled to $(S_a, S_{c,1})$.

The Hamiltonian of a BCS superconductor is the following:

$$\mathcal{H}_{BCS} = -W \sum_{\langle i,j \rangle} \sum_{\sigma_z=\uparrow,\downarrow} (c_{i,\sigma_z}^+ c_{j,\sigma_z} + c_{j,\sigma_z}^+ c_{i,\sigma_z}) \quad (4)$$

$$- |\Delta| \sum_i \left(\exp(i\varphi_i) c_{i,\uparrow}^+ c_{i,\downarrow}^+ + \exp(-i\varphi_i) c_{i,\downarrow} c_{i,\uparrow} \right), \quad (5)$$

where $\sum_{\langle i,j \rangle}$ denotes summation over pairs of neighboring tight-binding sites labeled by i and j , and σ_z is the component of the spin along quantization axis. The bulk hopping amplitude is denoted by W and the notation $|\Delta|$ is used for the superconducting gap, identical in all superconducting leads S_a , S_b , $S_{c,1}$ and $S_{c,2}$. The variable φ_i denotes the superconducting phase variable at the tight-binding site labeled by i . In the following, the current is weak and φ_i is approximated as being uniform in space, with the values φ_a , φ_b , $\varphi_{c,1}$, and $\varphi_{c,2}$ in S_a , S_b , $S_{c,1}$ and $S_{c,2}$ respectively.

We assume short distance between the contact points c_1 and c_2 (at the interfaces between $S_{c,1}$ or $S_{c,2}$ and the quantum dot), see figure 1j. We use the approximation of the gauge

$$\varphi_{c,1} = \varphi_c \quad (6)$$

$$\varphi_{c,2} = \varphi_c + \Phi, \quad (7)$$

where Φ is the flux enclosed in the loop terminated by $S_{c,1}$ and $S_{c,2}$.

The Hamiltonian of the tight-binding quantum dot on fig-

ure 1j is given by

$$\mathcal{H}_{dot} = -W \sum_{\langle i,j \rangle} \sum_{\sigma_z=\uparrow,\downarrow} (c_{i,\sigma_z}^+ c_{j,\sigma_z} + c_{j,\sigma_z}^+ c_{i,\sigma_z}) \quad (8)$$

$$- \mu_{dot} \sum_i \sum_{\sigma=\uparrow,\downarrow} c_{i,\sigma}^+ c_{i,\sigma}, \quad (9)$$

where μ_{dot} is the quantum dot chemical potential and the hopping amplitude W is chosen as identical to Eq. (4). The following circuit-model calculations are qualitative, and they do not rely on the type of lattice, *e.g.* square or hexagonal lattice as long as large gate-voltage value avoids the specific effects of the Dirac cones in the graphene dispersion relation.

Part of the following discussion is based on the phenomenological quantum dot circuit models on figures 1k and 1m. The Hamiltonian of a zero-dimensional (0D) quantum dot at location \mathbf{x} is the following

$$\mathcal{H}_{\mathbf{x},0D} = \varepsilon_x \sum_{\sigma_z} c_{\mathbf{x},\sigma_z}^+ c_{\mathbf{x},\sigma_z}, \quad (10)$$

where ε_x is the on-site energy. Similarly, the double quantum dot Hamiltonian is characterized by the on-site energies ε_x and ε_y with tunneling amplitude $\Sigma^{(1)}$ between them:

$$\mathcal{H}_{\mathbf{y},0D} = \varepsilon_y \sum_{\sigma_z} c_{\mathbf{y},\sigma_z}^+ c_{\mathbf{y},\sigma_z} \quad (11)$$

$$\mathcal{H}_{T,1} = -\Sigma^{(1)} \sum_{\sigma_z} c_{\mathbf{x},\sigma_z}^+ c_{\mathbf{y},\sigma_z} + h.c., \quad (12)$$

see also Eq. (79) in the Appendix.

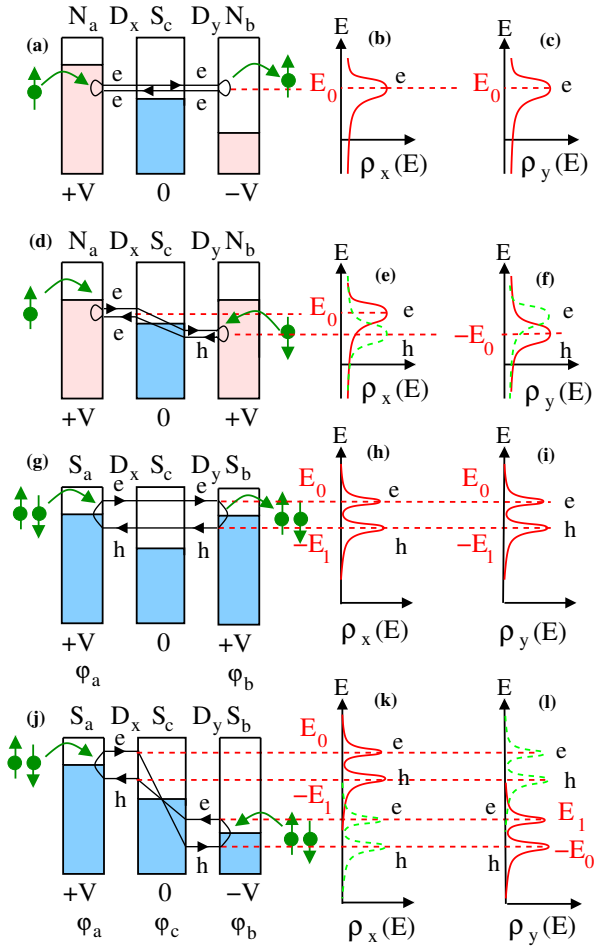


FIG. 3. *The nonlocal resonances.* Panels a, d, g and j show the lowest-order diagrams of elastic cotunneling (EC), crossed Andreev reflection (CAR), double elastic cotunneling (dEC) and double crossed Andreev reflection (dCAR) respectively. Panels b, e, h and k show the energy- E -dependence of the density of states $\rho_x(E)$ on the quantum dot D_x and panels c, f, i and l show the corresponding $\rho_y(E)$ on the quantum dot D_y . Panels e, f, k and l also show for completeness by green dashed lines the complementary resonances that do not directly contribute to the corresponding transport processes.

In order to make correspondence between the populations of the ballistic device and the single or double quantum dot circuits on figures 1k and 1m, the quantum dot reference energy is chosen to be shifted by the chemical potential of the ballistic metal. At small temperature, the populations cross-over from “occupied” if the energy ω is such that $\omega \lesssim \mu_{dot}$ to “empty” if $\omega \gtrsim \mu_{dot}$. This mimics the energy-dependence of the occupation number of a Fermi sea, on the condition that the chemical potential μ_{dot} is such that $\mu_{dot} = E_F$, where the ballistic metal Fermi energy E_F is practically chosen as the energy-reference.

The tunneling Hamiltonian depends on the time variable t , and transfers single-particle states between the quantum dot and the superconducting leads:

$$\mathcal{H}_{T,0} = -\Sigma^{(0)} \sum_{j,\sigma_z} \exp(-i\omega_0 t) c_{j,\sigma_z}^+ c_{j',\sigma_z} + h.c., \quad (13)$$

where $\Sigma^{(0)}$ is the hopping amplitude. The summation in Eq. (13) runs over the pairs of sites (j, j') on both sides of the interface, and $\omega_0 = eV/\hbar$ is set by the voltage drop.

The degree of “proximitization” of the ballistic metal is expected to depend on whether the ballistic conductor is 2D or 3D. Considering the 2D metal-based device on figure 1, the “cross” formed in between the superconductors ($S_a, S_b, S_{c,1}, S_{c,2}$) is not expected to be proximitized, and this is the physical origin of the normal leads in our model.

The Hamiltonian of a normal lead is given by

$$\mathcal{H}_N = -W \sum_{\langle i,j \rangle} \sum_{\sigma_z=\uparrow,\downarrow} (c_{i,\sigma_z}^+ c_{j,\sigma_z} + c_{j,\sigma_z}^+ c_{i,\sigma_z}) \quad (14)$$

$$-\mu_N \sum_i \sum_{\sigma=\uparrow,\downarrow} c_{i,\sigma}^+ c_{i,\sigma}, \quad (15)$$

where μ_N is the normal lead chemical potential and the hopping amplitude W is chosen as identical to Eq. (4).

The following subsections IV A, IV B and IV C analytically demonstrate our claims on the anomalously large value of the quartet current and its specific voltage dependence on the basis of microscopic Green’s functions calculations based on the above BCS Hamiltonians given by Eq. (4)-(5), the quantum dot Hamiltonian given by Eqs. (8)-(9), the normal-lead Hamiltonian given by Eq. (14) and tunneling between them, see Eq. (13). Subsection IV D introduces the circuit models that are used in the numerical calculations of section V. Those circuits models are phenomenological. They have no other justification than containing the ingredients for the resonances and relaxation, with feasible computation times that, otherwise, are more demanding for the devices on figures 1j and figure 2a. In addition, the circuit model C on figure 2b naturally becomes exact if the lattice shown on figure 2a contains only two two tight-binding sites. On figure 2b, both quantum dots D_x and D_y are connected by hopping amplitudes to the “auxiliary” tight-binding sites $a, b, c_1, c_2, \alpha_x, \beta_x, \alpha_y, \beta_y$ to which the green-colored local and nonlocal Green’s functions are connected. In addition, the lower tunneling path on figure 2b features the possibility that the spin-up electrons and spin-down holes can cross one of the normal leads while the upper tunneling path shows direct propagation between α_x and α_y across the quantum dot. Overall, the circuit on figure 2b is used to mimic the two-path interference shown on figure 2a, see the forthcoming section IV D for how model C on figure 2b is mapped onto model D.

IV. ANALYTICAL RESULTS

This section presents analytical results on the interplay between nonlocal Andreev resonances and relaxation.

Subsection IV A discusses non-Hermitian effective Hamiltonian in the infinite-gap limit. Subsections IV B and IV C present how anomalously large values of the quartet critical current emerge from the rotating wave approximation. The reduction to simple circuit is discussed in subsection IV D.

A. Emergence of non-Hermitian effective Hamiltonian

In this subsection, we discuss emergence of non-Hermitian effective Hamiltonians for a finite-size quantum dot coupled to normal and superconducting leads, and biased on the quartet line, see figures 1j and 2a.

The four-terminal Josephson junction is captured by a tight-binding lattice of finite dimension, see figures 1j and 2a. This “quantum dot” is coupled to s superconducting leads labeled by $\sigma = 1, \dots, s$ and to n normal leads labeled by $v = 1, \dots, n$. The Dyson equations take the form

$$\begin{aligned} \hat{G}_{D,D} &= \hat{g}_{D,D} + \sum_{v=1}^n \hat{g}_{D,D} \hat{\Sigma}_{D,N_v}^{(0)} \hat{g}_{N_v,N_v} \hat{\Sigma}_{N_v,D}^{(0)} \hat{G}_{D,D} \quad (16) \\ &+ \sum_{\sigma=1}^s \hat{g}_{D,D} \hat{\Sigma}_{D,S_{\sigma}}^{(0)} \hat{g}_{S_{\sigma},S_{\sigma}} \hat{\Sigma}_{S_{\sigma},D}^{(0)} \hat{G}_{D,D}, \end{aligned}$$

where \hat{g}_{N_v,N_v} and $\hat{g}_{S_{\sigma},S_{\sigma}}$ are the bare Green’s functions of the normal or superconducting leads N_v or S_{σ} respectively, and $\hat{g}_{D,D}$ and $\hat{G}_{D,D}$ are the bare and fully dressed quantum dot Green’s functions, with

$$\hat{g}_{D,D,x,y}^{A,1,1} = \sum_p \langle x|p \rangle \frac{1}{\omega - \varepsilon_p - i\eta} \langle p|y \rangle \quad (17)$$

$$\hat{g}_{D,D,x,y}^{A,2,2} = \sum_p \langle x|p \rangle \frac{1}{\omega + \varepsilon_p - i\eta} \langle p|y \rangle, \quad (18)$$

where “1, 1” and “2, 2” refer to the electron-electron and hole-hole channels respectively. The notation $|p\rangle$ stands for the single-particle states, and $\langle x|p \rangle$, $\langle y|p \rangle$ are the corresponding wave-functions at the tight-binding sites x and y . The notations $\hat{\Sigma}_{D,N_v}^{(0)}$ or $\hat{\Sigma}_{D,S_{\sigma}}^{(0)}$ in Eq. (16) refer to the hopping amplitudes from the dot to the normal or superconducting leads, and $\hat{\Sigma}_{N_v,D}^{(0)}$ or $\hat{\Sigma}_{S_{\sigma},D}^{(0)}$ correspond to hopping from the normal or superconducting leads to the quantum dot. The bare and fully dressed Green’s functions $\hat{g}_{D,D}$ and $\hat{G}_{D,D}$ have entries in the Nambu labels, and in the tight-binding sites at the contacts between the dot and the normal or superconducting leads N_v or S_{σ} . In addition, those matrices have entries in the set of the harmonics of the Josephson frequency. The Dynes parameter η in Eqs. (17)-(18) [89–92] makes the distinction between the advanced and retarded Green’s functions, and it can be used to capture relaxation on the quantum dot [46].

Eq. (16) is rewritten as

$$\begin{aligned} &\left[\hat{g}_{D,D}^{-1} - \sum_{v=1}^n \hat{\Sigma}_{D,N_v}^{(0)} \hat{g}_{N_v,N_v} \hat{\Sigma}_{N_v,D}^{(0)} - \sum_{\sigma=1}^s \hat{\Sigma}_{D,S_{\sigma}}^{(0)} \hat{g}_{S_{\sigma},S_{\sigma}} \hat{\Sigma}_{S_{\sigma},D}^{(0)} \right] \times \\ &\hat{G}_{D,D} = \hat{I}. \quad (19) \end{aligned}$$

Now, we extend the domain of definition of the Dyson equations from the interfaces to the entire tight-binding lattice. The resolvent of the quantum dot Hamiltonian is given by the retarded Green’s function:

$$\hat{g}_{D,D}^R = (\omega + i\eta - \hat{\mathcal{H}}_{dot})^{-1}, \quad (20)$$

where $\hat{\mathcal{H}}_{dot}$ is the quantum dot Hamiltonian, see Eqs. (8)-(9) in section III. We consider in addition that $\hat{g}_{S,S}$ is independent

on ω , which is deduced from the infinite-gap limit, and that \hat{g}_{N_v,N_v} is also independent on energy. The infinite-gap limit was introduced and considered over the last few years, see for instance Refs. 80, 94, and 95 to cite but a few. The resolvent takes the form

$$\hat{G}_{D,D}^R = \left(\omega + i\eta - \hat{\mathcal{H}}_{eff}^{(\infty)} \right)^{-1}, \quad (21)$$

where the infinite-gap-limit Hamiltonian

$$\begin{aligned} \hat{\mathcal{H}}_{eff}^{(\infty)} &= \hat{\mathcal{H}}_{D,D} + \sum_{v=1}^n \hat{\Sigma}_{D,N_v}^{(0)} \hat{g}_{N_v,N_v} \hat{\Sigma}_{N_v,D}^{(0)} \quad (22) \\ &+ \sum_{\sigma=1}^s \hat{\Sigma}_{D,S_{\sigma}}^{(0)} \hat{g}_{S_{\sigma},S_{\sigma}} \hat{\Sigma}_{S_{\sigma},D}^{(0)} \end{aligned}$$

is non-Hermitian, due to \hat{g}_{N_v,N_v} .

B. Rotating wave approximation

Now, we discuss the rotating wave approximation in the case of the infinite-gap limit Hamiltonian given by Eq. (22), see the Supplemental Material of Ref. 46 for a three-terminal 0D quantum dot with $\hat{g}_{N_v,N_v} = 0$. As in the preceding subsection IV A, we consider here finite-size quantum dot coupled to normal and superconducting leads, and biased on the quartet line, see figures 1j and 2a.

We define the quantum state $|\psi(t)\rangle$ at time t as the superposition

$$|\psi(t)\rangle = \sum_p \alpha_p(t) |\psi_p(t)\rangle \quad (23)$$

of the eigenstates $|\psi_p(t)\rangle$, such that

$$\hat{\mathcal{H}}_{eff}^{(\infty)}(t) |\psi_p(t)\rangle = \varepsilon_p(t) |\psi_p(t)\rangle. \quad (24)$$

We deduce

$$\begin{aligned} i \frac{d\alpha_q(t)}{dt} &= \alpha_q(t) \left\{ \varepsilon_q(t) - i \langle \psi_q(t) \frac{d|\psi_q(t)\rangle}{dt} \right\} \quad (25) \\ &- i \sum_{p \neq q} \alpha_p(t) \langle \psi_q(t) \frac{d|\psi_p(t)\rangle}{dt} \rangle. \end{aligned}$$

The Rabi resonances are at the voltages

$$2eV_{p,q} = \varepsilon_p - \varepsilon_q, \quad (26)$$

with $p \neq q$, and where $\varepsilon_p = \langle \varepsilon_p(t) \rangle$, $\varepsilon_q = \langle \varepsilon_q(t) \rangle$ denote the time-averaged energies in Eq. (24). In addition, we assume that the period of oscillations is much shorter than the relaxation time and the imaginary part of ε_p and ε_q can then be discarded. Both ε_p and ε_q are sensitive on the magnetic flux Φ through the loop, see figure 1a. Thus, the corresponding resonant voltages $V_{p,q}(\Phi)$ are Φ -sensitive. The set of the $V_{p,q}(\Phi = 0)$ values can be interdigitated with $V_{p,q}(\Phi = \pi)$, which implies nontrivial dependence of $I_{q,c}(\Phi = \pi, eV/\Delta) - I_{q,c}(\Phi = 0, eV/\Delta)$ as a function of the bias voltage V , see also our previous paper II [51] for a four-terminal single 0D quantum dot.

The quartet critical current $I_{q,c}$ is defined as the amplitude of variations of the quartet current as a function of the quartet phase. In addition, the numerical calculations of section V evaluate the antisymmetric combinations

$$I_{q,c}(\Phi = 0, eV/\Delta) = \dots \quad (27)$$

$$\max_{\varphi_q} [I_q(\Phi = 0, \varphi_q, eV/\Delta) - I_q(\Phi = 0, -\varphi_q, eV/\Delta)]$$

$$- \min_{\varphi_q} [I_q(\Phi = 0, \varphi_q, eV/\Delta) - I_q(\Phi = 0, -\varphi_q, eV/\Delta)]$$

$$I_{q,c}(\Phi = \pi, eV/\Delta) = \dots \quad (28)$$

$$\max_{\varphi_q} [I_q(\Phi = \pi, \varphi_q, eV/\Delta) - I_q(\Phi = \pi, -\varphi_q, eV/\Delta)]$$

$$- \min_{\varphi_q} [I_q(\Phi = \pi, \varphi_q, eV/\Delta) - I_q(\Phi = \pi, -\varphi_q, eV/\Delta)].$$

C. Diverging current response

In this subsection, we evaluate the quartet current at resonance and show that it can exceed by orders of magnitude the maximal supercurrent $2e\Delta/\hbar$ through a single-channel weak link connecting two superconductors, see for instance Refs. 96 and 97 for the current through a single-channel weak link. Again, in this subsection, the device consists of a finite-size quantum dot coupled to normal and superconducting leads, and biased on the quartet line, see figures 1j and 2a.

The current flowing from the multilevel quantum dot into the superconducting lead S_σ is given by the following energy-integral [97, 98]:

$$I_{D,S_\sigma} = \frac{e}{\hbar} \int d\omega \times \quad (29)$$

$$\text{Tr} \left[\hat{\sigma}^z \left\{ \hat{\Sigma}_{D,S_\sigma}^{(0)} \hat{G}_{S_\sigma,D}^{+,-} - \hat{\Sigma}_{S_\sigma,D}^{(0)} \hat{G}_{D,S_\sigma}^{+,-} \right\} \right],$$

where the Pauli matrix $\hat{\sigma}^z$ is defined as $\hat{\sigma}^z = \text{diag}(1, -1)$ on the set of the Nambu labels. In the infinite-gap limit $\hat{g}_{\lambda,\lambda'}^{+,-} \neq 0$ if λ, λ' belong to a normal lead. We focus on the first term $\hat{\Sigma}_{D,S_\sigma}^{(0)} \hat{G}_{S_\sigma,D}^{+,-}$ appearing in Eq. (29), the second term being treated similarly:

$$\hat{\Sigma}_{D,S_\sigma}^{(0)} \hat{G}_{S_\sigma,D}^{+,-} = \quad (30)$$

$$\sum_{\lambda, \lambda'} \hat{\Sigma}_{D,S_\sigma}^{(0)} \left[\hat{I} + \hat{G}^R \hat{\Sigma}^{(0)} \right]_{S_\sigma, \lambda} \hat{g}_{\lambda, \lambda'}^{+,-} \left[\hat{I} + \hat{\Sigma}^{(0)} \hat{G}^A \right]_{\lambda', D},$$

where λ, λ' run over the N_V -side of the interface between the quantum dot and the normal lead N_V . Eq. (30) yields

$$\hat{\Sigma}_{D,S_\sigma}^{(0)} \hat{G}_{S_\sigma,D}^{+,-} = \sum_{\lambda, \lambda'} \hat{\Sigma}_{D,S_\sigma}^{(0)} \times \quad (31)$$

$$\sum_{\mu, \mu'} \hat{g}_{S_\sigma, S_\sigma}^R \hat{\Sigma}_{S_\sigma, \mu}^{(0)} \hat{G}_{\mu, \mu'}^R \hat{\Sigma}_{\mu', \lambda}^{(0)} \times$$

$$\hat{g}_{\lambda, \lambda'}^{+,-} \sum_{\tilde{\mu}, \tilde{\mu}'} \hat{\Sigma}_{\lambda', \tilde{\mu}}^{(0)} \hat{G}_{\tilde{\mu}, \tilde{\mu}'}^A \hat{\Sigma}_{\tilde{\mu}', D}^{(0)} \hat{g}_{D,D}^A.$$

The fully dressed Green's functions are approximated as [47,

77]

$$\hat{G}_{\mu, \mu'}^{R,1,2}(\omega) \simeq \frac{\hat{\mathcal{R}}_{\mu, \mu', l, \tau}}{\omega + 2leV + \tau\Omega_{i_0} + i\delta_{i_0}} \quad (32)$$

$$\hat{G}_{\tilde{\mu}, \tilde{\mu}'}^{A,2,1}(\omega) \simeq \frac{\hat{\mathcal{R}}'_{\tilde{\mu}, \tilde{\mu}', \tilde{l}, \tilde{\tau}}}{\omega + 2\tilde{l}eV + \tilde{\tau}\Omega_{i_0} - i\delta_{i_0}}, \quad (33)$$

where $\hat{\mathcal{R}}_{\mu, \mu', l, \tau}$ and $\hat{\mathcal{R}}'_{\tilde{\mu}, \tilde{\mu}', \tilde{l}, \tilde{\tau}}$ are the matrix residues, δ_{i_0} is the line-width broadening, l and \tilde{l} are two integers and $\tau, \tilde{\tau} = \pm 1$. Rabi resonances are obtained for

$$\omega + 2leV + \tau\Omega_{i_0} = \omega + 2\tilde{l}eV + \tilde{\tau}\Omega_{i_0}, \quad (34)$$

with the first resonance at $eV = \Omega_{i_0}$.

Integrating the above Eqs. (30)-(31) over ω , and using the expressions of $\hat{G}_{\mu, \mu'}^{R,1,2}(\omega)$ and $\hat{G}_{\tilde{\mu}, \tilde{\mu}'}^{A,2,1}(\omega)$ [see the above Eqs. (32)-(33)], yields the scaling form $I_{D,S_\sigma} \sim 1/\delta_{i_0}$ of the quartet current at the resonant voltage value $eV = \Omega_{i_0}$, that can thus exceed $2e\Delta/\hbar$ by orders of magnitude. This is in agreement with the preceding Eq. (3) in the above section II, see also the numerical calculations presented in the forthcoming section V.

This diverging current response is also in agreement with the strong effect on the current of tiny quantum dot Dynes parameter $\eta_D = 0^+$ in comparison with $\eta_D = 0$, regarding two-level quantum dots, see section IID in the Supplemental Material of Ref. 46.

We underline that, in Eq. (30), $\hat{g}_{\mu, \mu'}^{+,-} = 0$ if μ, μ' belong to a superconducting lead treated in the infinite-gap limit. Thus, the resonance $I_{D,S_\sigma} \sim 1/\delta_{i_0}$ in the current is not operational in absence of “extrinsic” relaxation by the normal leads attached to the quantum dot.

D. Equivalence between models C and D

Now, we propose mechanism for emergence of complex effective tunneling amplitudes, and we consider the simple phenomenological circuit models on figure 2.

We note that tunneling between the superconducting leads S_σ and $S_{\sigma'}$ is the result of interference between the “direct” path $S_\sigma \rightarrow \text{dot} \rightarrow S_{\sigma'}$ across the finite-size tight-binding quantum dot, and “indirect” one $S_\sigma \rightarrow \text{dot} \rightarrow N_V \rightarrow \text{dot} \rightarrow S_{\sigma'}$ that involves the normal lead N_V . This interference provides complex-valued nonlocal Green's functions connecting pairs of superconducting leads, and a finite value for the nonlocal density of states and $\hat{g}_{\lambda, \lambda'}^{+,-}$ in the above Eqs. (30)-(31).

The interfering tunneling paths are shown on figure 2a, and the corresponding circuit model C is presented on figure 2b. The labels are made explicit on this figure, regarding the quantum dots D_x and D_y , the tight-binding sites and the hopping amplitudes.

In addition, we implicitly assume that summing over the channels labeled by λ and λ' does not result in complete destructive interference in the current given by the above Eqs. (30)-(31), due to the finite size of the quantum dot used for the region of the junction.

Figure 2c features equivalence with model D containing effective complex-valued path connecting the tight-binding sites α and β .

Now, we provide the details of the calculations by which model D on figure 2c is deduced from model C on figure 2b.

The Dyson equation associated to model C on figure 2 takes the form

$$\begin{aligned}\hat{G}_{D_x, D_x} &= \hat{g}_{D_x, D_x} + \hat{g}_{D_x, D_x} \hat{\Gamma}_{D_x, D_x}^{S_a, S_a} \hat{G}_{D_x, D_x} + \hat{g}_{D_x, D_x} \hat{\Gamma}_{D_x, D_x}^{S_{c_1}, S_{c_1}} \hat{G}_{D_x, D_x} + \hat{g}_{D_x, D_x} \hat{\Gamma}_{D_x, D_x}^{\alpha_x, \alpha_x} \hat{G}_{D_x, D_x} + \hat{g}_{D_x, D_x} \hat{\Gamma}_{D_x, D_x}^{\beta_x, \beta_x} \hat{G}_{D_x, D_x} \\ &+ \hat{g}_{D_x, D_x} \hat{\Gamma}_{D_x, D_y}^{\alpha_x, \alpha_y} \hat{G}_{D_y, D_x} + \hat{g}_{D_x, D_x} \hat{\Gamma}_{D_x, \delta_x}^{\beta_x, \beta'_x} \hat{G}_{\delta_x, D_x}\end{aligned}\quad (35)$$

$$\hat{G}_{\delta_x, D_x} = \hat{g}_{\delta_x, \delta_x} \hat{\Gamma}_{\delta_x, \delta_x}^{\beta'_x, \beta'_x} \hat{G}_{\delta_x, D_x} + \hat{g}_{\delta_x, \delta_x} \hat{\Gamma}_{\delta_x, D_x}^{\beta'_x, \beta_x} \hat{G}_{D_x, D_x} + \hat{g}_{\delta_x, \delta_x} \hat{\Gamma}_{\delta_x, \delta_y}^{\beta'_x, \beta'_y} \hat{G}_{\delta_y, D_x} + \hat{g}_{\delta_x, \delta_x} \hat{\Gamma}_{\delta_y, D_x}^{\beta'_y, \beta_x} \hat{G}_{D_y, D_x} \quad (36)$$

$$\hat{G}_{\delta_y, D_x} = \hat{g}_{\delta_y, \delta_x} \hat{\Gamma}_{\delta_x, \delta_x}^{\beta'_x, \beta'_x} \hat{G}_{\delta_x, D_x} + \hat{g}_{\delta_y, \delta_x} \hat{\Gamma}_{\delta_x, D_x}^{\beta'_x, \beta_x} \hat{G}_{D_x, D_x} + \hat{g}_{\delta_y, \delta_y} \hat{\Gamma}_{\delta_y, \delta_y}^{\beta'_y, \beta'_y} \hat{G}_{\delta_y, D_x} + \hat{g}_{\delta_y, \delta_y} \hat{\Gamma}_{\delta_y, D_x}^{\beta'_y, \beta_x} \hat{G}_{D_y, D_x} \quad (37)$$

$$\hat{G}_{D_y, D_x} = \hat{g}_{D_y, D_x} \hat{\Gamma}_{D_y, D_x}^{\alpha_y, \alpha_x} \hat{G}_{D_x, D_x} + \hat{g}_{D_y, D_x} \hat{\Gamma}_{D_y, D_x}^{\alpha_y, \alpha_y} \hat{G}_{D_y, D_x} + \hat{g}_{D_y, D_x} \hat{\Gamma}_{D_y, D_y}^{\beta_y, \beta_y} \hat{G}_{D_y, D_x} + \hat{g}_{D_y, D_x} \hat{\Gamma}_{D_y, \delta_y}^{\beta_y, \beta'_y} \hat{G}_{\delta_y, D_x}, \quad (38)$$

where $\hat{\Gamma}_{i,j}^{k,l} = \hat{\sigma}_{i,k} \hat{g}_{k,l} \hat{\sigma}_{l,j}$. Eqs. (35)-(38) are rewritten as

$$\begin{aligned}\hat{G}_{D_x, D_x} &= \hat{g}_{D_x, D_x} + \hat{g}_{D_x, D_x} \hat{\Gamma}_{D_x, D_x}^{S_a, S_a} \hat{G}_{D_x, D_x} + \hat{g}_{D_x, D_x} \hat{\Gamma}_{D_x, D_x}^{S_{c_1}, S_{c_1}} \hat{G}_{D_x, D_x} + \hat{g}_{D_x, D_x} \hat{\Gamma}_{D_x, D_x}^{\alpha_x, \alpha_x} \hat{G}_{D_x, D_x} + \hat{g}_{D_x, D_x} \hat{\Gamma}_{D_x, D_x}^{\beta_x, \beta_x} \hat{G}_{D_x, D_x} \\ &+ \hat{g}_{D_x, D_x} \hat{\Gamma}_{D_x, D_y}^{\alpha_x, \alpha_y} \hat{G}_{D_y, D_x} + \hat{g}_{D_x, D_x} \hat{\Gamma}_{D_x, \delta_x}^{\beta_x, \beta'_x} \left(\hat{E}_{\delta_x, D_x} \hat{G}_{D_x, D_x} + \hat{E}_{\delta_x, D_y} \hat{G}_{D_y, D_x} \right)\end{aligned}\quad (39)$$

$$\begin{aligned}\hat{G}_{D_y, D_x} &= \hat{g}_{D_y, D_x} \hat{\Gamma}_{D_y, D_x}^{\alpha_y, \alpha_x} \hat{G}_{D_x, D_x} + \hat{g}_{D_y, D_x} \hat{\Gamma}_{D_y, D_x}^{\alpha_y, \alpha_y} \hat{G}_{D_y, D_x} + \hat{g}_{D_y, D_x} \hat{\Gamma}_{D_y, D_y}^{\beta_y, \beta_y} \hat{G}_{D_y, D_x} \\ &+ \hat{g}_{D_y, D_x} \hat{\Gamma}_{D_y, \delta_y}^{\beta_y, \beta'_y} \left(\hat{E}_{\delta_y, D_x} \hat{G}_{D_x, D_x} + \hat{E}_{\delta_y, D_y} \hat{G}_{D_y, D_x} \right),\end{aligned}\quad (40)$$

where

$$\hat{E}_{\delta_x, D_x} = \left[\hat{I} - \hat{A}_{\delta_x, \delta_x} - \hat{A}_{\delta_x, \delta_y} \left(\hat{I} - \hat{A}_{\delta_y, \delta_y} \right)^{-1} \hat{A}_{\delta_y, \delta_x} \right]^{-1} \times \left[\hat{D}_{\delta_x, D_x} + \hat{A}_{\delta_x, \delta_y} \left(\hat{I} - \hat{A}_{\delta_y, \delta_y} \right)^{-1} \hat{D}_{\delta_y, \delta_x} \right] \quad (41)$$

$$\hat{E}_{\delta_x, D_y} = \left[\hat{I} - \hat{A}_{\delta_x, \delta_x} - \hat{A}_{\delta_x, \delta_y} \left(\hat{I} - \hat{A}_{\delta_y, \delta_y} \right)^{-1} \hat{A}_{\delta_y, \delta_x} \right]^{-1} \times \left[\hat{D}_{\delta_x, D_y} + \hat{A}_{\delta_x, \delta_y} \left(\hat{I} - \hat{A}_{\delta_y, \delta_y} \right)^{-1} \hat{D}_{\delta_y, \delta_y} \right] \quad (42)$$

$$\hat{E}_{\delta_y, D_x} = \left(\hat{I} - \hat{A}_{\delta_y, \delta_y} \right)^{-1} \times \left[\hat{A}_{\delta_y, \delta_x} \hat{E}_{\delta_x, D_x} + \hat{D}_{\delta_y, D_x} \right] \quad (43)$$

$$\hat{E}_{\delta_y, D_y} = \left(\hat{I} - \hat{A}_{\delta_y, \delta_y} \right)^{-1} \times \left[\hat{A}_{\delta_y, \delta_x} \hat{E}_{\delta_x, D_y} + \hat{D}_{\delta_y, D_y} \right], \quad (44)$$

with $\hat{A}_{\delta_x, \delta_x} = \hat{g}_{\delta_x, \delta_x} \hat{\sigma}_{\delta_x} \hat{g}_{\beta'_x, \beta'_x} \hat{\sigma}_{\delta_x}$, $\hat{A}_{\delta_x, \delta_y} = \hat{g}_{\delta_x, \delta_y} \hat{\sigma}_{\delta_y} \hat{g}_{\beta'_y, \beta'_y} \hat{\sigma}_{\delta_y}$, $\hat{A}_{\delta_y, \delta_x} = \hat{g}_{\delta_y, \delta_x} \hat{\sigma}_{\delta_x} \hat{g}_{\beta'_x, \beta'_x} \hat{\sigma}_{\delta_x}$, $\hat{A}_{\delta_y, \delta_y} = \hat{g}_{\delta_y, \delta_y} \hat{\sigma}_{\delta_y} \hat{g}_{\beta'_y, \beta'_y} \hat{\sigma}_{\delta_y}$ and $\hat{D}_{\delta_x, D_x} = \hat{g}_{\delta_x, \delta_x} \hat{\Gamma}_{\delta_x, D_x}^{\beta'_x, \beta_x}$, $\hat{D}_{\delta_x, D_y} = \hat{g}_{\delta_x, \delta_y} \hat{\Gamma}_{\delta_x, D_y}^{\beta'_x, \beta_y}$, $\hat{D}_{\delta_y, D_x} = \hat{g}_{\delta_y, \delta_x} \hat{\Gamma}_{\delta_x, D_x}^{\beta'_x, \beta_x}$, $\hat{D}_{\delta_y, D_y} = \hat{g}_{\delta_y, \delta_y} \hat{\Gamma}_{\delta_y, D_y}^{\beta'_y, \beta_y}$. Equivalently,

$$\hat{G}_{D_x, D_x} = \hat{g}_{D_x, D_x} + \hat{g}_{D_x, D_x} \hat{\Gamma}'_{D_x, D_x} \hat{G}_{D_x, D_x} + \hat{g}_{D_x, D_x} \hat{\Gamma}'_{D_x, D_y} \hat{G}_{D_y, D_x} \quad (45)$$

$$\hat{G}_{D_y, D_x} = \hat{g}_{D_y, D_x} \hat{\Gamma}'_{D_y, D_x} \hat{G}_{D_x, D_x} + \hat{g}_{D_y, D_x} \hat{\Gamma}'_{D_y, D_y} \hat{G}_{D_y, D_x}, \quad (46)$$

with

$$\hat{\Gamma}'_{D_x, D_x} = \hat{\Gamma}_{D_x, D_x}^{S_a, S_a} + \hat{\Gamma}_{D_x, D_x}^{S_{c_1}, S_{c_1}} + \hat{\Gamma}_{D_x, D_x}^{\alpha_x, \alpha_x} + \hat{\Gamma}_{D_x, D_x}^{\beta_x, \beta_x} + \hat{\Gamma}_{D_x, \delta_x}^{\beta_x, \beta'_x} \hat{E}_{\delta_x, D_x} \quad (47)$$

$$\hat{\Gamma}'_{D_x, D_y} = \hat{\Gamma}_{D_x, D_y}^{\alpha_x, \alpha_y} + \hat{\Gamma}_{D_x, \delta_x}^{\beta_x, \beta'_y} \hat{E}_{\delta_x, D_y} \quad (48)$$

$$\hat{\Gamma}'_{D_y, D_x} = \hat{\Gamma}_{D_y, D_x}^{\alpha_y, \alpha_x} + \hat{\Gamma}_{D_y, \delta_y}^{\beta_y, \beta'_x} \hat{E}_{\delta_y, D_x} \quad (49)$$

$$\hat{\Gamma}'_{D_y, D_y} = \hat{\Gamma}_{D_y, D_y}^{\alpha_y, \alpha_y} + \hat{\Gamma}_{D_y, \delta_y}^{\beta_y, \beta_y} + \hat{\Gamma}_{D_y, \delta_y}^{\beta_y, \beta'_y} \hat{E}_{\delta_y, D_y}, \quad (50)$$

where \hat{E} is complex-valued matrix.

We deduce the phenomenological circuit model D on figure 2c: the Green's functions colored in yellow on figure 2c

take the form

$$\hat{g}_{\alpha, \beta}^{1,1} = \hat{g}_{\beta, \alpha}^{1,1} = \alpha_R + i\alpha_I \quad (51)$$

$$\hat{g}_{\alpha, \beta}^{2,2} = \hat{g}_{\beta, \alpha}^{2,2} = -\alpha_R + i\alpha_I \quad (52)$$

$$\hat{g}_{\alpha, \alpha}^{1,1} = \hat{g}_{\beta, \beta}^{1,1} = \beta_R + i\beta_I \quad (53)$$

$$\hat{g}_{\alpha, \alpha}^{2,2} = \hat{g}_{\beta, \beta}^{2,2} = -\beta_R + i\beta_I, \quad (54)$$

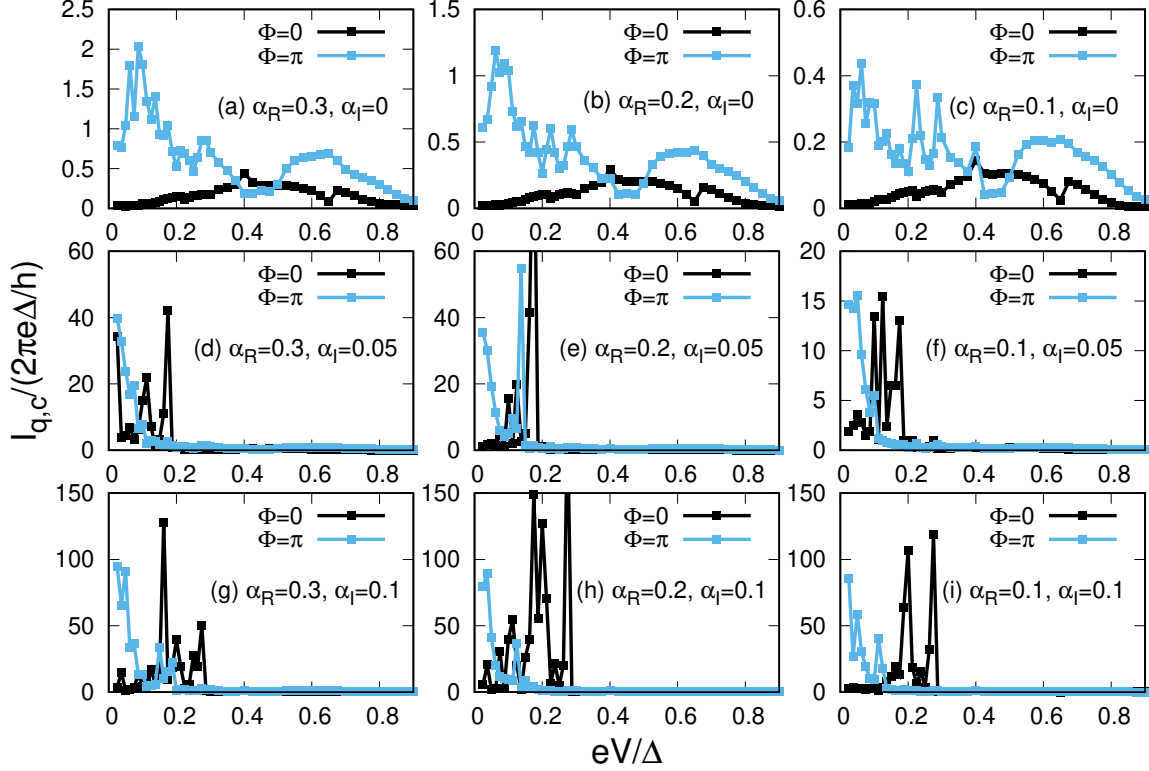


FIG. 4. The eV/Δ -dependence of the quartet critical current. Each panel of this figure shows $I_{q,c}(eV/\Delta, \Phi = 0)$ and $I_{q,c}(\Phi = \pi, eV/\Delta)$ as a function of the normalized bias voltage eV/Δ , for $\alpha_I = 0$ and $\alpha_R = 0.3/W$ (a), $\alpha_R = 0.2/W$ (b) and $\alpha_R = 0.1/W$ (c). Panels d, e and f correspond to $\alpha_I = 0.05/W$ and $\alpha_R = 0.3/W$ (d), $\alpha_R = 0.2/W$ (e) and $\alpha_R = 0.1/W$ (f) and panels g, h, i show $I_{q,c}(\Phi = 0, eV/\Delta)$ and $I_{q,c}(\Phi = \pi, eV/\Delta)$ for $\alpha_I = 0.1/W$ and $\alpha_R = 0.3/W$ (g), $\alpha_R = 0.2/W$ (h) and $\alpha_R = 0.1/W$ (i). We use $\Gamma/\Delta = 1$, $\Gamma'/\Delta = 0$, $\beta_R = \beta_I = 0$, and $\varepsilon_x = \varepsilon_y = 0$. The notation W is used for the band-width.

where (α_R, α_I) , and (β_R, β_I) are four real-valued parameters for the nonlocal and local Green's functions $\hat{g}_{\alpha,\beta} = \hat{g}_{\beta,\alpha}$ and $\hat{g}_{\alpha,\alpha} = \hat{g}_{\beta,\beta}$ respectively.

In order to further justify Eqs. (51)-(54), we denote by $|p\rangle$ the states of the multilevel quantum dot connected to normal leads, in absence of coupling to the superconductors. The retarded Green's function encoding propagation between the tight-binding sites \mathbf{x} and \mathbf{y} is given by

$$g_{\mathbf{x} \rightarrow \mathbf{y}}^R = \sum_p \langle \mathbf{x} | p \rangle \frac{\omega - \varepsilon_p - i\eta_0}{(\omega - \varepsilon_p)^2 + \eta_0^2} \langle p | \mathbf{y} \rangle, \quad (55)$$

which leads to

$$\text{Re}[g_{\mathbf{x} \rightarrow \mathbf{y}}^R] \quad (56)$$

$$= \sum_p \frac{\text{Re}[\langle \mathbf{x} | p \rangle \langle p | \mathbf{y} \rangle] (\omega - \varepsilon_p) + \text{Im}[\langle \mathbf{x} | p \rangle \langle p | \mathbf{y} \rangle] \eta_0}{(\omega - \varepsilon_p)^2 + \eta_0^2}$$

$$\text{Im}[g_{\mathbf{x} \rightarrow \mathbf{y}}^R] \quad (57)$$

$$= \sum_p \frac{\text{Im}[\langle \mathbf{x} | p \rangle \langle p | \mathbf{y} \rangle] (\omega - \varepsilon_p) + \text{Re}[\langle \mathbf{x} | p \rangle \langle p | \mathbf{y} \rangle] \eta_0}{(\omega - \varepsilon_p)^2 + \eta_0^2}.$$

Similarly,

$$\text{Re}[g_{\mathbf{y} \rightarrow \mathbf{x}}^R] \quad (58)$$

$$= \sum_p \frac{\text{Re}[\langle \mathbf{x} | p \rangle \langle p | \mathbf{y} \rangle] (\omega - \varepsilon_p) - \text{Im}[\langle \mathbf{x} | p \rangle \langle p | \mathbf{y} \rangle] \eta_0}{(\omega - \varepsilon_p)^2 + \eta_0^2}$$

$$\text{Im}[g_{\mathbf{y} \rightarrow \mathbf{x}}^R] \quad (59)$$

$$= \sum_p \frac{-\text{Im}[\langle \mathbf{x} | p \rangle \langle p | \mathbf{y} \rangle] (\omega - \varepsilon_p) + \text{Re}[\langle \mathbf{x} | p \rangle \langle p | \mathbf{y} \rangle] \eta_0}{(\omega - \varepsilon_p)^2 + \eta_0^2}.$$

Considering time-reversal symmetry (for instance such as with the plane-wave states $|p\rangle = |\mathbf{k}\rangle$ and $|p'\rangle = |-\mathbf{k}\rangle$), we obtain

$$\text{Im}[\langle \mathbf{x} | p \rangle \langle p | \mathbf{y} \rangle + \langle \mathbf{x} | p' \rangle \langle p' | \mathbf{y} \rangle] = 0, \quad (60)$$

from what we deduce

$$\text{Re}[g_{\mathbf{x} \rightarrow \mathbf{y}}^R] = \text{Re}[g_{\mathbf{y} \rightarrow \mathbf{x}}^R] \quad (61)$$

$$= \sum_p \frac{\text{Re}[\langle \mathbf{x} | p \rangle \langle p | \mathbf{y} \rangle] (\omega - \varepsilon_p)}{(\omega - \varepsilon_p)^2 + \eta_0^2}$$

$$\text{Im}[g_{\mathbf{x} \rightarrow \mathbf{y}}^R] = \text{Im}[g_{\mathbf{y} \rightarrow \mathbf{x}}^R] = \sum_p \frac{\text{Re}[\langle \mathbf{x} | p \rangle \langle p | \mathbf{y} \rangle] \eta_0}{(\omega - \varepsilon_p)^2 + \eta_0^2}. \quad (62)$$

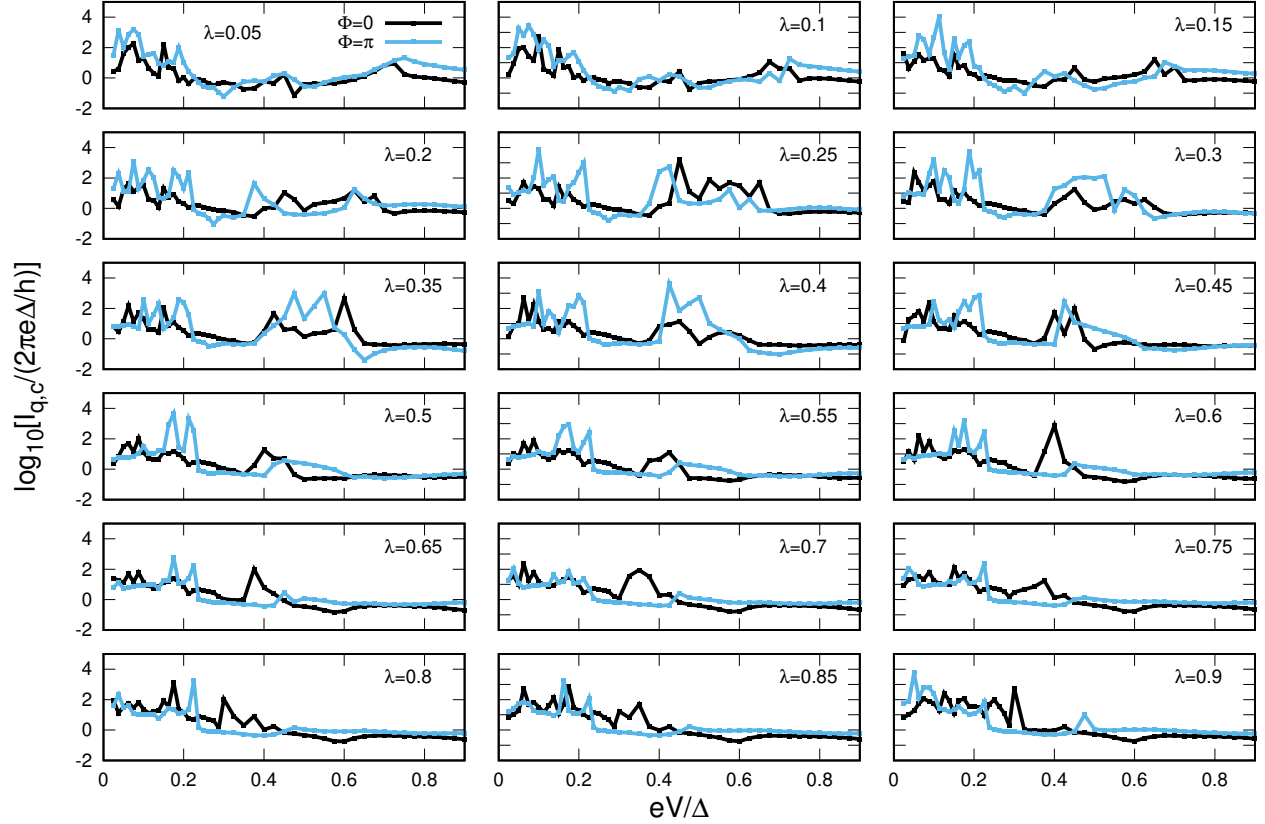


FIG. 5. The eV/Δ -dependence of the quartet critical current. The figure shows the reduced voltage- eV/Δ -dependence of the quartet critical currents $I_{q,c}(\Phi = 0, eV/\Delta)$ and $I_{q,c}(\Phi = \pi, eV/\Delta)$ at $\Phi = 0$ and $\Phi = \pi$ respectively. The panels show increasing values of $\lambda = \Gamma'/\Gamma$, where the couplings Γ and Γ' are schematically shown on figure 1m. We used $\Gamma/\Delta = 1$, $\alpha_R = 0.3/W$, $\alpha_I = 0.05/W$, and $\beta_R = \beta_I = 0$, where W is the band-width. The on-site energies $\varepsilon_x = \varepsilon_y = 0$ are vanishingly small.

In addition, we note that $g_{2,2}^A = 1/[\omega + \mathcal{H} - i\eta_0]$ is related to $g_{1,1}^R = 1/[\omega - \mathcal{H} + i\eta_0]$ by the relation $g_{2,2}^A(\omega) = -g_{1,1}^R(-\omega)$, where \mathcal{H} is the Hamiltonian of the “quantum dot coupled to normal leads”, see section III. We conclude that the previous Eqs. (51)-(54) have been demonstrated.

We additionally assume on a phenomenological basis that α_R , α_I , β_R and β_I are energy-independent. This assumption does not preclude emergence of energy-dependent Green’s functions of the coupled double quantum dot, since each individual quantum dot D_x or D_y has energy-dependent Green’s function.

Now that we defined the circuit model D by figure 2c, see also Eqs. (51)-(54), we present the corresponding numerical calculations that confirm the preceding discussion.

V. NUMERICAL RESULTS

In this section, we present selection of the numerical results based on the phenomenological circuit model D on figure 2,

see also Eqs. (51)-(54). Overall, those numerical calculations illustrate that relaxation produces anomalously large quartet current $I_{q,c} \gg 2e\Delta/\hbar$ in a four-terminal Josephson junction where S_a and S_b are biased at $\pm V$, and the grounded $S_{c,1}$ and $S_{c,2}$ are connected by a loop pierced by the magnetic flux Φ . In addition, small characteristic voltage scale V_* emerges in the variations of the quartet current with voltage.

The codes have been developed over the last few years [45–47, 51, 54, 58, 60, 77]. They are based on recursive calculations as a function of the harmonics of the Josephson frequency [96, 97] (see also the Appendix of Ref. 45) and on sparse matrix algorithms for matrix products. We specifically use the same code as in our recent Ref. 54, specializing to the relevant values of the local and nonlocal Green’s functions given by Eqs. (51)-(54).

We successively present the voltage-dependence of the quartet critical current $I_{q,c}$ defined by the above Eqs. (27)-(28) (see figures 4 and 5) and colormaps for the sign of $I_{q,c}$ as a function of the model parameters (see figures 6 and 7).

Figure 4 shows the normalized bias voltage eV/Δ

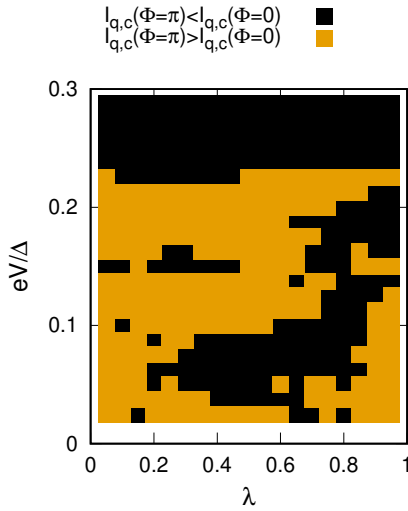


FIG. 6. *The sign of the inversion.* The figure shows the sign of $I_{q,c}(\lambda, \Phi = \pi, eV/\Delta) - I_{q,c}(\lambda, \Phi = 0, eV/\Delta)$, where $\lambda = \Gamma'/\Gamma$. Inversion corresponds to $I_{q,c}(\lambda, \Phi = \pi, eV/\Delta) - I_{q,c}(\lambda, \Phi = 0, eV/\Delta) > 0$. The parameter Γ is the “direct” coupling between D_x and $(S_a, S_{c,1})$ or between D_y and $(S_b, S_{c,2})$. The parameter Γ' is in between D_x and $(S_b, S_{c,2})$ or D_y and $(S_a, S_{c,1})$, see figure 1m. We used $\Gamma/\Delta = 1$, $\alpha_R = 0.3/W$, $\alpha_I = 0.05/W$, and $\beta_R = \beta_I = 0$, where W is the band-width. The on-site energies $\varepsilon_x = \varepsilon_y = 0$ are vanishingly small.

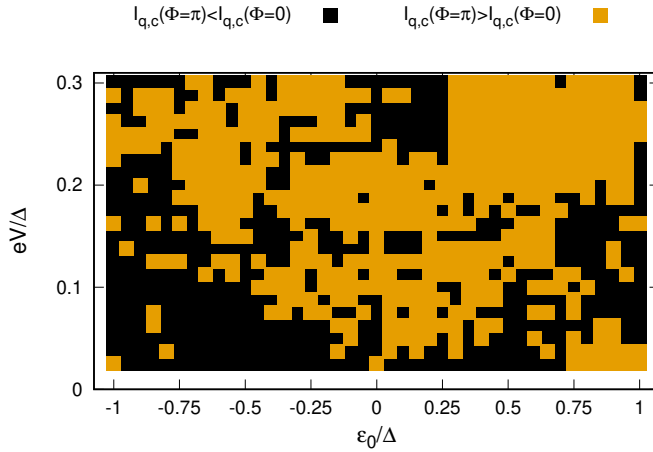


FIG. 7. *The sign of the inversion.* The figure is similar to the previous figure 6, but now the sign of $I_{q,c}(\varepsilon_0/\Delta, \Phi = \pi, eV/\Delta) - I_{q,c}(\varepsilon_0/\Delta, \Phi = 0, eV/\Delta)$ is shown in the $(\varepsilon_0/\Delta, eV/\Delta)$ plane. We used $\Gamma/\Delta = 1$, $\alpha_R = 0.3/W$, $\alpha_I = 0.05/W$, $\beta_R = \beta_I = 0$ (where W is the band-width) and $\lambda = \Gamma'/\Gamma = 1/2$. The on-site energies are identical for both quantum dots: $\varepsilon_x = \varepsilon_y = \varepsilon_0$.

dependence of the quartet critical currents $I_{q,c}(\Phi = 0, eV/\Delta)$ and $I_{q,c}(\Phi = \pi, eV/\Delta)$ at the flux values $\Phi = 0$ and $\Phi = \pi$. The coupling parameters $\Gamma/\Delta = 1$ and $\Gamma' = 0$ are used on figure 4. The notation Γ stands for the normal-state line-width broadening associated to tunneling between the quantum dot D_x and $(S_a, S_{c,1})$ or between the quantum dot D_y and $(S_b, S_{c,2})$, see figure 1m. The coupling Γ' corresponds to tunneling between D_x and $(S_b, S_{c,2})$, or between D_y and $(S_a, S_{c,1})$.

Figures 4a, 4b and 4c correspond to absence of relaxation with $\alpha_I = 0$, producing small quartet critical current $I_{q,c} < 2e\Delta/\hbar$. Figures 4d, 4e, 4f and 4g, 4h, 4i correspond to the finite relaxation parameters $\alpha_I = 0.05/W$ and $\alpha_I = 0.1/W$ respectively, producing large quartet critical current $I_{q,c} \gg 2e\Delta/\hbar$ at small voltage ratio eV/Δ . In addition, sharp resonances emerge for $\alpha_I = 0.05/W$ and $\alpha_I = 0.1/W$ on figures 4d, 4e, 4f and 4g, 4h, 4i respectively, in the variations of the quartet critical current as a function of eV/Δ . These numerical results on figure 4 are in agreement with the analytical calculations presented in section IV.

Figure 5 shows the normalized voltage- eV/Δ -dependence of the quartet critical current $I_{q,c}$, in semi-logarithmic scale, now with nonvanishingly small $\lambda = \Gamma'/\Gamma$ and $\alpha_I = 0.05/W$. The quartet critical current $I_{q,c}$ exceeds $2e\Delta/\hbar$ by orders of magnitude on figure 5. In addition, multiple cross-overs are obtained between $I_{q,c}(\Phi = \pi, eV/\Delta) - I_{q,c}(\Phi = 0, eV/\Delta) > 0$ (i.e. inversion) and $I_{q,c}(\Phi = \pi, eV/\Delta) - I_{q,c}(\Phi = 0, eV/\Delta) < 0$ (i.e. noninverted behavior) in a low-voltage window.

Figure 6 shows the sign of $I_{q,c}(\lambda, \Phi = \pi, eV/\Delta) - I_{q,c}(\lambda, \Phi = 0, eV/\Delta)$ as a function of the parameters $\lambda = \Gamma'/\Gamma$ (on the x-axis) and eV/Δ (on the y-axis). Inversion $I_{q,c}(\lambda, \Phi = \pi, eV/\Delta) - I_{q,c}(\lambda, \Phi = 0, eV/\Delta) > 0$ is obtained at low eV/Δ for $\lambda = 0$, see the Appendix for a discussion of the $eV/\Delta = 0^+$ limit. On figure 6, increasing the coupling Γ' between D_x and $(S_b, S_{c,2})$ or between D_y and $(S_a, S_{c,1})$ [in addition to Γ between D_x and $(S_a, S_{c,1})$ or between D_y and $(S_b, S_{c,2})$], makes the double quantum dot behave closer to a pair of single quantum dots. This favors the “noninverted behavior” typical of single quantum dots, as opposed to the “inverted behavior” appearing at $\lambda = \Gamma'/\Gamma = 0$ in a double quantum dot, see the Appendix.

Figure 7 shows the effect of gating away from particle-hole symmetry, in the presence of finite on-site energies $\varepsilon_x = \varepsilon_y \equiv \varepsilon_0$. The parameter $\lambda = \Gamma'/\Gamma$ is set to $\lambda = 1/2$ on figure 7. The data for $\lambda = 1/2$ on figure 6 match those on figure 7 for $\varepsilon_0/\Delta = 0$. Moving away from $\varepsilon_0 = 0$ on figure 7 produces typical voltage-dependence of $I_{q,c}(\lambda, \Phi = \pi, eV/\Delta) - I_{q,c}(\lambda, \Phi = 0, eV/\Delta)$ with “noninverted behavior” at low $V < V_*$ and “inversion” at higher $V > V_*$, see for instance the moderately small values $-0.5 \lesssim \varepsilon_0/\Delta \lesssim 0.5$ on figure 7. With the considered parameters, the ratio eV_*/Δ is in the range $eV_*/\Delta \approx 0.1$, thus being qualitatively compatible with the Harvard group experiment [60], see the forthcoming section VI.

VI. DISCUSSION

Now, we focus on discussing our results from the point of view of an additional argument for emergence of $I_{q,c} \gg 2e\Delta/\hbar$, see subsection VI A. Relevance to the recent Harvard group experiment is next suggested in subsection VI B.

A. Additional argument for $I_{q,c} \gg 2e\Delta/\hbar$

We start with the double quantum dot on figure 1m in the simple limit where the four superconducting leads are discon-

neted, i.e. $\Gamma = \Gamma' = 0$. We deal with the two quantum dots D_x and D_y connected to the tight-binding sites α and β by the tunneling amplitudes $\Sigma_{x,\alpha}^{(0)} = \Sigma_{\alpha,x}^{(0)}$ and $\Sigma_{y,\beta}^{(0)} = \Sigma_{\beta,y}^{(0)}$. The tight-binding sites are self-connected by the Green's functions $g_{\alpha,\alpha}$ and $g_{\beta,\beta}$, and connected to each other by the nonlocal Green's functions $g_{\alpha,\beta} = g_{\beta,\alpha}$. We denote by $g_{x,x}^A = g_{y,y}^A = 1/(\omega - i\eta)$ the Green's functions of the “isolated” quantum dots D_x and D_y , see Eqs. (10)(10) with $\varepsilon_x = \varepsilon_y = 0$. In addition $\tilde{g}_{x,x}$, $\tilde{g}_{y,y}$ are their counterparts for the connected double quantum dot, and by $\tilde{g}_{x,y}$ and $\tilde{g}_{y,x}$ are the corresponding nonlocal Green's functions. The Dyson equations relate the g s to the \tilde{g} s according to

$$\tilde{g}_{x,x} = g_{x,x} + g_{x,x}\Sigma_{x,\alpha}^{(0)}g_{\alpha,\alpha}\Sigma_{\alpha,x}^{(0)}\tilde{g}_{x,x} \quad (63)$$

$$+ g_{x,x}\Sigma_{x,\alpha}^{(0)}g_{\alpha,\beta}\Sigma_{\beta,y}^{(0)}\tilde{g}_{y,x}$$

$$\tilde{g}_{y,x} = g_{y,y}\Sigma_{y,\beta}^{(0)}g_{\beta,\alpha}\Sigma_{\alpha,x}^{(0)}\tilde{g}_{x,x} + g_{y,y}\Sigma_{y,\beta}^{(0)}g_{\beta,\beta}\Sigma_{\beta,y}^{(0)}\tilde{g}_{y,x}, \quad (64)$$

which leads to the secular equation

$$\begin{vmatrix} \omega - \Gamma_{x,\alpha,\alpha,x} & -\Gamma_{x,\alpha,\beta,y} \\ -\Gamma_{y,\beta,\alpha,x} & \omega - \Gamma_{y,\beta,\beta,y} \end{vmatrix} = 0, \quad (65)$$

where $\Gamma_{x,\alpha,\alpha,x} = \Sigma_{x,\alpha}^{(0)}g_{\alpha,\alpha}\Sigma_{\alpha,x}^{(0)}$, $\Gamma_{y,\beta,\beta,y} = \Sigma_{y,\beta}^{(0)}g_{\beta,\beta}\Sigma_{\beta,y}^{(0)}$, $\Gamma_{x,\alpha,\beta,y} = \Sigma_{x,\alpha}^{(0)}g_{\alpha,\beta}\Sigma_{\beta,y}^{(0)}$, $\Gamma_{y,\beta,\alpha,x} = \Sigma_{y,\beta}^{(0)}g_{\beta,\alpha}\Sigma_{\alpha,x}^{(0)}$. Assuming symmetric contacts yields $\Gamma_{x,\alpha,\alpha,x} = \Gamma_{y,\beta,\beta,y} \equiv \Gamma_{loc}$ and $\Gamma_{x,\alpha,\beta,y} = \Gamma_{y,\beta,\alpha,x} \equiv \Gamma_{nonloc}$. The energy levels are given by

$$\omega_{(\pm)} = \Gamma_{loc} \pm \Gamma_{nonloc} \quad (66)$$

$$= \left(\Sigma^{(0)} \right)^2 [\beta_R \pm \alpha_R] + i \left(\Sigma^{(0)} \right)^2 [\beta_I \pm \alpha_I], \quad (67)$$

where α_R , α_I , β_R and β_I are given by Eqs. (51)-(54).

Assuming tunnel coupling between the superconductors and the double quantum dot, a quartet created at time $t = 0$ in the state

$$|\mathcal{Q}(0)\rangle = c_{\omega_{(+),\uparrow}}^+(0)c_{\omega_{(+),\downarrow}}^+(0)c_{\omega_{(-),\uparrow}}^+(0)c_{\omega_{(-),\downarrow}}^+(0) \quad (68)$$

freely evolves according to

$$|\mathcal{Q}(t)\rangle = \exp(-i\mathcal{H}_{dot}t)|\mathcal{Q}(0)\rangle \quad (69)$$

$$= \exp[-2i(\text{Re}(\omega_{(+)}) + \text{Re}(\omega_{(-)}))t] \times \quad (70)$$

$$\exp[2(\text{Im}(\omega_{(+)}) + \text{Im}(\omega_{(-)}))t]|\mathcal{Q}(0)\rangle.$$

Now, we assume $\beta_R = \beta_I = 0$, as in the previous section V. Then, Eqs. (66)-(67) yield energy levels $\omega_{(\pm)} = \pm \Sigma^{(0)}(\alpha_R + i\alpha_I)$ having opposite real and imaginary parts, as it is expected for non-Hermitian Hamiltonians, see section IV A. Eqs. (69)-(70) become static:

$$|\mathcal{Q}(t)\rangle = |\mathcal{Q}(0)\rangle, \quad (71)$$

with the coupling to the normal leads producing absence of relaxation and dephasing of the quartet state. This strong quartet proximity effect is compatible with emergence of large quartet current $I_{q,c} \gg 2e\Delta/\hbar$.

Conversely, the single-level 0D quantum dots of our previous paper II [51] would produce absence of the quartet proximity effect, i.e. $|\mathcal{Q}(0)\rangle = 0$. This explains why four-terminal double quantum dots with extrinsic relaxation by normal carriers are proposed here as “minimal models” for the split quartets, instead of the four-terminal single 0D quantum dots of our previous paper II [51].

B. Possible relevance to experiments

Now, we point out the possibility of connection between our theory and the recent Harvard group experiment [60] on graphene-based four-terminal Josephson junctions.

Our previous theoretical papers I and II [50, 51] are summarized in section I of the Supplemental Material [93].

We first summarize the main features of the experiment [60], which implements the device on figure 1a corresponding to four superconducting leads (S_a , S_b , $S_{c,1}$, $S_{c,2}$) evaporated on a sheet of ballistic graphene. The $S_{c,1}$ and $S_{c,2}$ terminals are defined as both ends of the superconducting loop S_c pierced by the magnetic flux Φ . The superconducting leads S_a and S_b are biased at the voltages V_a and V_b , and S_c is grounded. The experiment [60] reports dc-Josephson-like anomaly on the $V_a + V_b \simeq 0$ line, which is compatible with the theory of the quartets [42–55]. The experimental quartet critical current $I_{q,c}(\Phi, eV/\Delta)$ is sensitive to both values of the magnetic flux Φ and the voltage V , in a way that is sketched in figure 1b. Change of sign from $I_{q,c}(\Phi = \pi, eV/\Delta) - I_{q,c}(\Phi = 0, eV/\Delta) < 0$ for $V < V_*$ to $I_{q,c}(\Phi = \pi, eV/\Delta) - I_{q,c}(\Phi = 0, eV/\Delta) > 0$ for $V > V_*$ is experimentally found [60], i.e. change of sign between “noninverted” and “inverted” as the bias voltage increases from $V < V_*$ to $V > V_*$. The experimental V_* is such that $eV_* \approx \Delta/10$.

Now, we suggest compatibility between our model and the recent experimental results of Ref. 60, see the above figure 1b sketching non inverted-to-inverted cross-over in the experimental $I_{q,c}(\Phi = \pi, eV/\Delta) - I_{q,c}(\Phi = 0, eV/\Delta)$ as a function of the voltage V .

Namely, we first clarify the “question mark” on figure 1c, i.e. the choice of simple model that contains the relevant physical ingredients. In the remaining of the paper, we focus on what we call the models A and B, and show that they can be ruled out as candidates for being compatible with the voltage-sensitivity of the experimental signal [60], see figure 1b because they do not produce small voltage, contrary to the two-Cooper pair resonances considered above within the above models C and D.

We start the discussion with two limiting cases: In model A, the four superconducting leads are weakly coupled to infinite ballistic 2D metal, and, in model B, they are weakly coupled to 2D ballistic normal region in the short-junction limit. “Short-junction limit” means that the sheet of graphene below the superconducting leads is proximitized, and “superconducting lead + graphene underneath” is treated as bulk BCS superconductor. In addition, we assume in model B that the region of the sheet of graphene in between the contacts is short compared to $\hbar v_F/\Delta$, where v_F is the Fermi velocity of

the graphene layer.

Figures 1d-1e feature the density of states of model A, taken as being or not energy-dependent. Figure 1f shows the gapped density of states of model B in the short-junction limit.

Three processes are taken into account within perturbation theory in the tunneling amplitudes between the superconducting and nonsuperconducting parts of the circuit: (i) The Q_1 quartets correspond to two Cooper pairs transmitted into the grounded $S_{c,1}$, from S_a and S_b biased at $V_{a,b} = \pm V$, see figure 1g; (ii) The Q_2 quartets are similar to the Q_1 quartets, but now the outgoing Cooper pairs are transmitted at the $S_{c,2}$ contact, see figure 1h; (iii) The SQ split quartets correspond to two Cooper pairs from $S_{a,b}$ that exchange a quasiparticle, and are separately transmitted into the grounded $S_{c,1}$ and $S_{c,2}$, see figure 1i.

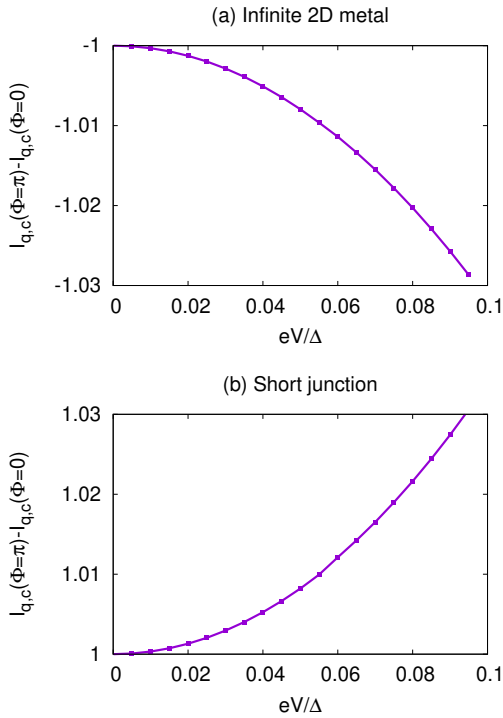


FIG. 8. *The perturbative calculation.* The figure shows the voltage- V -sensitivity of $I_{q,c}(\Phi = \pi, eV/\Delta) - I_{q,c}(\Phi = 0, eV/\Delta)$ for model A (panel a), and model B (panel b). The Dynes parameter is $\eta/\Delta = 10^{-2}$. Normalization is discussed in the text.

Now, we evaluate the bias voltage-sensitivity of the inversion within the above models A and B, a calculation that was not addressed in our preceding paper I [50].

The split-quartet diagrams at finite bias voltage are shown on figures 2c and 2d in the Supplemental Material [93].

We numerically implement Keldysh perturbation theory to evaluate the currents from the fully dressed Keldysh Green's function $\hat{G}^{+,-}$, see the Dyson-Keldysh Eqs. (1)-(5) in the Supplemental Material [93].

Figures 8a and 8b show the voltage-dependence of $I_{q,c}(\Phi = \pi, eV/\Delta) - I_{q,c}(\Phi = 0, eV/\Delta)$ for models A and B respectively, normalized such that $|I_{q,c}(\Phi = \pi, eV/\Delta) - I_{q,c}(\Phi = 0, eV/\Delta)|$ goes to unity in the $V = 0^+$ limit. The normalized

$I_{q,c}(\Phi = \pi, eV/\Delta) - I_{q,c}(\Phi = 0, eV/\Delta)$ in figures 8a and 8b is chosen to have the same sign as the unnormalized $I_{q,c}(\Phi = \pi, eV/\Delta) - I_{q,c}(\Phi = 0, eV/\Delta)$.

Figures 8a and 8b reveal that $I_{q,c}(\Phi = \pi, eV/\Delta) - I_{q,c}(\Phi = 0, eV/\Delta)$ has only weak sensitivity on the bias voltage V . Increasing the bias voltage V does not trigger change of sign in $I_{q,c}(\Phi = \pi, eV/\Delta) - I_{q,c}(\Phi = 0, eV/\Delta)$ as the bias voltage V increases through the $eV \lesssim \eta$ to $eV \gtrsim \eta$ cross-over, where η is the Dynes parameter [46, 89–92].

It is concluded that figures 8a and 8b contradict the sketch of the experimental data on figure 1b regarding change of sign in $I_{q,c}(\Phi = \pi, eV/\Delta) - I_{q,c}(\Phi = 0, eV/\Delta)$ as a function of V . This motivates introduction of the circuit model discussed in the paper, having small energy scales within the superconducting gap, that produce nontrivial voltage-dependence of the quartet signal. As an output of this circuit model, figure 7 reveals a robust parameter window where ‘absence of inversion’ is obtained at low $V < V_*$, crossing-over to ‘inversion’ for $V > V_*$, where the order of magnitude $eV_*/\Delta \approx 0.1$ is compatible with the experimental data.

VII. CONCLUSIONS

To conclude, we reduced a ballistic multiterminal Josephson junction to tight-binding model connected to superconducting and normal leads, which was further simplified into a phenomenological two-node circuit. This circuit model is characterized by complex Green's function between the quantum dots D_x and D_y , and by first and second-neighbor couplings between the dots and the four superconducting leads. In the considered model, the nonproximitized regions of the ballistic conductor yield the normal-metal continua that produce relaxation.

We found anomalously large quartet critical current $I_{q,c} \gg 2e\Delta/\hbar$ in calculations that account for both the time-periodic dynamics and relaxation. This conclusion was reached from intertwined analytical microscopic calculations, numerical calculations, and intuitive arguments. Emergence of anomalously large quartet current in those circuit model calculations is compatible with the experimental quartet signal being above detection threshold [60].

In addition, noninverted-to-inverted cross-over numerically emerges as the bias voltage increases, where ‘inversion’ means ‘larger quartet critical current at half flux-quantum $\Phi = \pi$ than in zero field at $\Phi = 0$ ’. The corresponding cross-over voltage V_* is small compared to the superconducting, typically $eV_* \approx \Delta/10$ with the parameters that we used in our calculations, which is compatible with the recent Harvard group experiment [60].

The interaction between theory and experiments in the field of multiterminal Josephson junctions [42–82] is at its early days. In view of the opportunity of future experiments to probe the Floquet spectrum with finite frequency noise, see our previous Ref. 47, it would be interesting to evaluate the noise spectral density for the here-considered two-node model. Going beyond two-node circuit models would also be interesting and we already started preliminary calculations

with four-nodes, 1D chains and 2D square lattice clusters.

ACKNOWLEDGEMENTS

The author wishes to thank K. Huang, Y. Ronen and P. Kim for stimulating discussions about their experiment. The author wishes to thank R. Danneau for useful discussions and comments on the manuscript, and F. Levy-Bertrand and her colleagues H. Cercellier, K. Hasselbach, M.A. Measson for useful remarks during an informal seminar on this topic. The author thanks the Infrastructure de Calcul Intensif et de Données (GRICAD) for use of the resources of the Mésocentre de Calcul Intensif de l'Université Grenoble-Alpes (CIMENT). The author acknowledges support from the French National Research Agency (ANR) in the framework of the Graphmon project (ANR-19-CE47-0007).

APPENDIX: $V = 0^+$ ADIABATIC LIMIT

In this Appendix, we examine the $V = 0^+$ adiabatic limit of four-terminal Josephson junctions containing a single or two nodes (see subsections 1 and 2 below).

1. Single quantum dot

We start with single 0D quantum dots in the $V = 0^+$ adiabatic limit, summarizing a fraction of the Supplemental Material of our previous paper II [51].

The Dyson Eqs. (4)-(5) in the Supplemental Material [93] are specialized to the considered 0D quantum dot connected to s superconducting leads by the tunnel amplitudes $\hat{\Sigma}_\sigma^{(0)}$, with $\sigma = 1, \dots, s$:

$$\hat{G}_{x,x} = \hat{g}_{x,x} + \hat{g}_{x,x} \sum_{\sigma=1}^s \hat{\Sigma}_{x,S_\sigma}^{(0)} \hat{g}_{S_\sigma, S_\sigma} \hat{\Sigma}_{S_\sigma, x}^{(0)} \hat{G}_{x,x}. \quad (72)$$

In the infinite-gap limit, Eq. (72) can be expressed in terms of the infinite-gap Hamiltonian $\hat{\mathcal{H}}_\infty$:

$$\hat{G}_{x,x}^A = (\omega - i\eta - \hat{\mathcal{H}}_\infty)^{-1}, \quad (73)$$

where

$$\hat{\mathcal{H}}_\infty = \sum_{\sigma=1}^s \hat{\Sigma}_{x,S_\sigma}^{(0)} \hat{g}_{S_\sigma, S_\sigma} \hat{\Sigma}_{S_\sigma, x}^{(0)}. \quad (74)$$

Specifically, we obtain the following with $s = 4$ superconducting leads:

$$\hat{\mathcal{H}}_\infty = \begin{pmatrix} 0 & \gamma_{x,x} \\ (\gamma_{x,x})^* & 0 \end{pmatrix}, \quad (75)$$

where

$$\gamma_{x,x} = \Gamma_a \exp(i\varphi_a) + \Gamma_b \exp(i\varphi_b) \quad (76)$$

$$+ \Gamma_{c,1} \exp(i\varphi_{c,1}) + \Gamma_{c,2} \exp(i\varphi_{c,2}),$$

and $\Gamma_\sigma = (\Sigma_{x,S_\sigma})^2/W$ parameterizes the line-width broadening of the quantum dot level in the normal state.

The $(S_{c,1}, S_{c,2})$ superconducting leads can be gathered into the single $S_{c,eff}$ coupled by

$$\Gamma_{c,eff} = \Gamma_{c,1} \exp(i\varphi_{c,1}) + \Gamma_{c,2} \exp(i\varphi_{c,2}). \quad (77)$$

Using the identical $\Gamma_{c,1} = \Gamma_{c,2} \equiv \Gamma_c$ and the gauge given by Eqs. (6)-(7) yields

$$\Gamma_{c,eff} = \Gamma_c [1 + \exp(i\Phi)] \exp(i\varphi_{c,1}). \quad (78)$$

It was shown in the Supplemental Material of our previous paper II [51] that nonsymmetric coupling to the superconducting leads can produce inversion between $\Phi = 0$ and $\Phi = \pi$ in the infinite-gap limit. But Eq. (78) implies $|\Gamma_{c,eff}| = 2\Gamma_c$ if $\Phi = 0$ and $\Gamma_{c,eff} = 0$ if $\Phi = \pi$ for symmetric couplings to the superconducting leads, *i.e.* the quartet current at $\Phi = \pi$ is vanishingly small, thus it is automatically smaller than at $\Phi = 0$.

2. Double quantum dot

In this subsection, we provide simple argument for emergence of inversion in the double quantum dot on figure 1m, in the limits $eV/\Delta = 0^+$ and $\Gamma' = 0$. We also provide a physical argument for emergence of noninverted behavior at finite Γ'/Γ .

The 4×4 infinite-gap double quantum dot Hamiltonian at $\Gamma' = 0$ is given by

$$\hat{\mathcal{H}}_\infty = \begin{pmatrix} 0 & \gamma_{x,x} & \Sigma^{(1)} & 0 \\ (\gamma_{x,x})^* & 0 & 0 & -\Sigma^{(1)} \\ \Sigma^{(1)} & 0 & 0 & \gamma_{y,y} \\ 0 & -\Sigma^{(1)} & (\gamma_{y,y})^* & 0 \end{pmatrix}, \quad (79)$$

with

$$\gamma_{x,x} = \Gamma_a \exp(i\varphi_a) + \Gamma_{c,1} \exp(i\varphi_{c,1}) \quad (80)$$

$$\gamma_{y,y} = \Gamma_b \exp(i\varphi_b) + \Gamma_{c,2} \exp(i\varphi_{c,2}). \quad (81)$$

Squaring the infinite-gap Hamiltonian given by Eq. (79) leads to

$$(\hat{\mathcal{H}}_\infty)^2 = \begin{pmatrix} |\gamma_{x,x}|^2 + (\Sigma^{(1)})^2 & 0 & 0 & -\Sigma^{(1)} [\gamma_{x,x} - \gamma_{y,y}] \\ 0 & |\gamma_{x,x}|^2 + (\Sigma^{(1)})^2 & \Sigma^{(1)} [(\gamma_{x,x})^* - (\gamma_{y,y})^*] & 0 \\ 0 & \Sigma^{(1)} [\gamma_{x,x} - \gamma_{y,y}] & |\gamma_{y,y}|^2 + (\Sigma^{(1)})^2 & 0 \\ -\Sigma^{(1)} [(\gamma_{x,x})^* - (\gamma_{y,y})^*] & 0 & 0 & |\gamma_{y,y}|^2 + (\Sigma^{(1)})^2 \end{pmatrix}, \quad (82)$$

which decouples into the following 2×2 blocks:

$$[\hat{\mathcal{H}}^2]_{2 \times 2}^{(1)} = \begin{pmatrix} |\gamma_{x,x}|^2 + (\Sigma^{(1)})^2 & -\Sigma^{(1)} [\gamma_{x,x} - \gamma_{y,y}] \\ -\Sigma^{(1)} [(\gamma_{x,x})^* - (\gamma_{y,y})^*] & |\gamma_{y,y}|^2 + (\Sigma^{(1)})^2 \end{pmatrix} \quad (83)$$

and

$$[\hat{\mathcal{H}}^2]_{2 \times 2}^{(2)} = \begin{pmatrix} |\gamma_{x,x}|^2 + (\Sigma^{(1)})^2 & \Sigma^{(1)} [(\gamma_{x,x})^* - (\gamma_{y,y})^*] \\ \Sigma^{(1)} [\gamma_{x,x} - \gamma_{y,y}] & |\gamma_{y,y}|^2 + (\Sigma^{(1)})^2 \end{pmatrix}. \quad (84)$$

Thus,

$$\gamma_{x,x} - \gamma_{y,y} = \Gamma_a \exp(i\varphi_a) + \Gamma_{c,1} \exp(i\varphi_{c,1}) \quad (85)$$

$$- \Gamma_b \exp(i\varphi_b) - \Gamma_{c,2} \exp(i\varphi_{c,2}) \quad (86)$$

and the coupling to the effective $S_{c,eff}$ is now given by the difference

$$\Gamma_{c,eff} = \Gamma_{c,1} \exp(i\varphi_{c,1}) - \Gamma_{c,2} \exp(i\varphi_{c,2}) \quad (87)$$

instead of the previous Eq. (77) for 0D quantum dot. Eq. (87) goes to

$$\Gamma_{c,eff}(\Phi) = \Gamma [1 - \exp(i\Phi)] \exp(i\varphi_{c,1}) \quad (88)$$

in the considered limit $\Gamma_{c,1} = \Gamma_{c,2} \equiv \Gamma$ of symmetric couplings. Thus, the interference $|\Gamma_{c,eff}|(\Phi = 0) = 0$ and $|\Gamma_{c,eff}|(\Phi = \pi) = 2\Gamma$ yields inversion between $\Phi = 0$ and $\Phi = \pi$ with symmetric coupling to the superconducting leads. This contrasts with absence of inversion for the single 0D quantum dot, see section 1 in this Appendix.

[1] J. Bardeen, L. N. Cooper, and J. R. Schrieffer, *Theory of Superconductivity*, Phys. Rev. **108**, 1175 (1957).

[2] N. K. Allsopp, V. C. Hui, C. J. Lambert, and S. J. Robinson, *Theory of the sign of multi-probe conductances for normal and superconducting materials*, J. Phys.: Condens. Matter **6**, 10475 (1994).

[3] J. M. Byers and M. E. Flatté, *Probing Spatial Correlations with Nanoscale Two-Contact Tunneling*, Phys. Rev. Lett. **74**, 306 (1995).

[4] J. Torrès and T. Martin, *Positive and negative Hanbury-Brown and Twiss correlations in normal metal-superconducting devices*, Eur. Phys. J. B **12**, 319 (1999).

[5] G. Deutscher and D. Feinberg, *Coupling superconducting-ferromagnetic point contacts by Andreev reflections*, Appl. Phys. Lett. **76**, 487 (2000).

[6] M. S. Choi, C. Bruder, and D. Loss, *Spin-dependent Josephson current through double quantum dots and measurement of entangled electron states*, Phys. Rev. B **62**, 13569 (2000).

[7] G. Falci, D. Feinberg, and F. W. J. Hekking, *Correlated tunneling into a superconductor in a multiprobe hybrid structure*, Europhys. Lett. **54**, 255 (2001).

[8] P. Recher, E. V. Sukhorukov, and D. Loss, *Andreev tunneling, Coulomb blockade, and resonant transport of nonlocal spin-entangled electrons*, Phys. Rev. B **63**, 165314 (2001).

[9] G. B. Lesovik, T. Martin, and G. Blatter, *Electronic entanglement in the vicinity of a superconductor*, Eur. Phys. J. B **24**, 287 (2001).

[10] R. Mélin and D. Feinberg, *Transport theory of multiterminal hybrid structures*, Eur. Phys. J. B **26**, 101 (2002).

[11] N. M. Chtchelkatchev, G. Blatter, G. B. Lesovik, and T. Martin, *Bell inequalities and entanglement in solid-state devices*, Phys. Rev. B **66**, 161320 (2002).

[12] R. Mélin and D. Feinberg, *Sign of the crossed conductances at a ferromagnet/superconductor/ferromagnet double interface*, Phys. Rev. B **70**, 174509 (2004).

[13] A. V. Lebedev, G. B. Lesovik, and G. Blatter, *Generating spin-entangled electron pairs in normal conductors using voltage pulses*, Phys. Rev. B **72**, 245314 (2005).

[14] K. V. Bayandin, G. B. Lesovik, and T. Martin, *Energy entanglement in normal metal-superconducting forks* Phys. Rev. B **74**, 085326 (2006).

[15] A. L. Yeyati, F. S. Bergeret, A. Martín-Rodero, and T. M. Klapwijk, *Entangled Andreev pairs and collective excitations in nanoscale superconductors*, Nature Phys. **3**, 455 (2007).

[16] D. Beckmann, H. B. Weber, and H. v. Löhneysen, *Evidence for crossed Andreev reflection in Superconductor-Ferromagnet hybrid structures*, Phys. Rev. Lett. **93**, 197003 (2004).

[17] S. Russo, M. Kroug, T. M. Klapwijk, and A. F. Morpurgo, *Ex-*

perimental observation of bias-dependent nonlocal Andreev reflection, Phys. Rev. Lett. **95**, 027002 (2005).

[18] P. Cadden-Zimansky and V. Chandrasekhar, *Nonlocal correlations in normal-metal superconducting systems*, Phys. Rev. Lett. **97**, 237003 (2006).

[19] D. Beckmann, H. B. Weber, and H. v. Löhneysen, *Negative four-terminal resistance as a probe of crossed Andreev reflection*, Appl. Phys. A **89**, 603 (2007).

[20] P. Cadden-Zimansky, Z. Jiang, and V. Chandrasekhar, *Charge imbalance, crossed Andreev reflection and elastic co-tunnelling in ferromagnet/superconductor/normal-metal structures*, New J. Phys. **9**, 116 (2007).

[21] L. Hofstetter, S. Csonka, J. Nygård, and C. Schönenberger, *Cooper pair splitter realized in a two-quantum-dot Y-junction*, Nature (London) **461**, 960 (2009).

[22] L. G. Herrmann, F. Portier, P. Roche, A. Levy Yeyati, T. Kontos, and C. Strunk, *Carbon nanotubes as Cooper pair beam splitters*, Phys. Rev. Lett. **104**, 026801 (2010).

[23] J. Wei and V. Chandrasekhar, *Positive noise cross-correlation in hybrid superconducting and normal-metal three-terminal devices*, Nat. Phys. **6**, 494 (2010).

[24] A. Das, Y. Ronen, M. Heiblum, D. Mahalu, A. V. Kretinin, and H. Shtrikman, *High-efficiency Cooper pair splitting demonstrated by two-particle conductance resonance and positive noise cross-correlation*, Nat. Commun. **3**, 1165 (2012).

[25] J. Schindele, A. Baumgartner, and C. Schönenberger, *Near-Unity Cooper Pair Splitting Efficiency*, Phys. Rev. Lett. **109**, 157002 (2012).

[26] J. Schindele, A. Baumgartner, R. Maurand, M. Weiss, and C. Schönenberger, *Nonlocal spectroscopy of Andreev bound states*, Phys. Rev. B **89**, 045422 (2014).

[27] Z. B. Tan, D. Cox, T. Nieminen, P. Lähteenmäki, D. Golubev, G. B. Lesovik, and P. J. Hakonen, *Cooper Pair Splitting by Means of Graphene Quantum Dots*, Phys. Rev. Lett. **114**, 096602 (2015).

[28] I. V. Borzenets, Y. Shimazaki, G. F. Jones, M. F. Craciun, S. Russo, M. Yamamoto, and S. Tarucha, *High Efficiency CVD Graphene-lead (Pb) Cooper Pair Splitter*, Sci. Rep. **6**, 23051 (2016).

[29] P. Pandey, R. Danneau, and D. Beckmann, *Ballistic Graphene Cooper Pair Splitter*, Phys. Rev. Lett. **126**, 147701 (2021).

[30] M. P. Anantram and S. Datta, *Current fluctuations in mesoscopic systems with Andreev scattering*, Phys. Rev. B **53**, 16390 (1996).

[31] P. Samuelsson and M. Büttiker, *Chaotic dot-superconductor analog of the Hanbury Brown–Twiss effect*, Phys. Rev. Lett. **89**, 046601 (2002).

[32] P. Samuelsson and M. Büttiker, *Semiclassical theory of current correlations in chaotic dot-superconductor systems*, Phys. Rev. B **66**, 201306 (R) (2002).

[33] J. Börlin, W. Belzig, and C. Bruder, *Full counting statistics of a superconducting beam splitter*, Phys. Rev. Lett. **88**, 197001 (2002).

[34] P. Samuelsson, E.V. Sukhorukov, and M. Büttiker, *Orbital entanglement and violation of Bell inequalities in mesoscopic conductors*, Phys. Rev. Lett. **91**, 157002 (2003).

[35] L. Faoro, F. Taddei, and R. Fazio, *Clauser-Horne inequality for electron-counting statistics in multiterminal mesoscopic conductors*, Phys. Rev. B **69**, 125326 (2004).

[36] G. Bignon, M. Houzet, F. Pistolesi, and F.W.J. Hekking, *Current-current correlations in hybrid superconducting and normal metal multiterminal structures*, Europhys. Lett. **67**, 110 (2004).

[37] R. Mélin, C. Benjamin, and T. Martin, *Positive cross correlations of noise in superconducting hybrid structures: Roles of interfaces and interactions*, Phys. Rev. B **77**, 094512 (2008).

[38] A. Freyn, M. Flöser and R. Mélin, *Positive current cross-correlations in a highly transparent normal-superconducting beam splitter due to synchronized Andreev and inverse Andreev reflections*, Phys. Rev. B **82**, 014510 (2010).

[39] D.S. Golubev and A.D. Zaikin, *Shot noise and Coulomb effects on nonlocal electron transport in normal-metal/superconductor/normal-metal heterostructures*, Phys. Rev. B **82**, 134508 (2010).

[40] M. Flöser, D. Feinberg and R. Mélin, *Absence of split pairs in cross correlations of a highly transparent normal metal-superconductor-normal metal electron-beam splitter*, Phys. Rev. B **88**, 094517 (2013).

[41] G. Michalek, B. R. Bulka, T. Domański, and K. I. Wysokiński, *Statistical correlations of currents flowing through a proximitized quantum dot*, Phys. Rev. B **101**, 235402 (2020).

[42] A. Freyn, B. Douçot, D. Feinberg, and R. Mélin, *Production of non-local quartets and phase-sensitive entanglement in a superconducting beam splitter*, Phys. Rev. Lett. **106**, 257005 (2011).

[43] T. Jonckheere, J. Rech, T. Martin, B. Douçot, D. Feinberg, and R. Mélin, *Multipair DC Josephson resonances in a biased all-superconducting bijunction*, Phys. Rev. B **87**, 214501 (2013).

[44] R. Mélin, D. Feinberg, and B. Douçot, *Partially resummed perturbation theory for multiple Andreev reflections in a short three-terminal Josephson junction*, Eur. Phys. J. B **89**, 67 (2016).

[45] R. Mélin, M. Sotto, D. Feinberg, J.-G. Caputo and B. Douçot, *Gate-tunable zero-frequency current cross-correlations of the quartet mode in a voltage-biased three-terminal Josephson junction*, Phys. Rev. B **93**, 115436 (2016).

[46] R. Mélin, J.-G. Caputo, K. Yang and B. Douçot, *Simple Floquet-Wannier-Stark-Andreev viewpoint and emergence of low-energy scales in a voltage-biased three-terminal Josephson junction*, Phys. Rev. B **95**, 085415 (2017).

[47] R. Mélin, R. Danneau, K. Yang, J.-G. Caputo, and B. Douçot, *Engineering the Floquet spectrum of superconducting multiterminal quantum dots*, Phys. Rev. B **100**, 035450 (2019).

[48] J.D. Pillet, V. Benzoni, J. Griesmar, J.-L. Smirr, and Ç.Ö. Girit, *Nonlocal Josephson Effect in Andreev Molecules* Nano Lett. **19**, 7138 (2019).

[49] V. Kornich, H.S. Barakov, and Yu.V. Nazarov, *Fine energy splitting of overlapping Andreev bound states in multiterminal superconducting nanostructures*, Phys. Rev. Research **1**, 033004 (2019).

[50] R. Mélin and B. Douçot, *Inversion in a four terminal superconducting device on the quartet line. I. Two-dimensional metal and the quartet beam splitter*, Phys. Rev. B **102**, 245435 (2020).

[51] R. Mélin and B. Douçot, *Inversion in a four terminal superconducting device on the quartet line. II. Quantum dot and Floquet theory*, Phys. Rev. B **102**, 245436 (2020).

[52] J.-D. Pillet, V. Benzoni, J. Griesmar, J.-L. Smirr, and Ç.Ö. Girit, *Scattering description of Andreev molecules*, SciPost Phys. Core **2**, 009 (2020).

[53] V. Kornich, H. S. Barakov and Yu. V. Nazarov, *Overlapping Andreev states in semiconducting nanowires: competition of 1D and 3D propagation*, Phys. Rev. B **101**, 195430 (2020).

[54] R. Mélin, *Ultralong-distance quantum correlations in three-terminal Josephson junctions*, Phys. Rev. B **104**, 075402 (2021).

[55] A. Melo, V. Fatemi and A.R. Akhmerov, *Multiplet supercurrent in Josephson tunneling circuits*, arXiv:2104.11239 (2021).

[56] A.H. Pfeffer, J.E. Duvauchelle, H. Courtois, R. Mélin, D. Fein-

berg, and F. Lefloch, *Subgap structure in the conductance of a three-terminal Josephson junction*, Phys. Rev. B **90**, 075401 (2014).

[57] E. Strambini, S. D'Ambrosio, F. Vischi, F.S. Bergeret, Yu.V. Nazarov, and F. Giazotto, *The ω -SQUIPT as a tool to phase-engineer Josephson topological materials*, Nat. Nanotechnol. **11**, 1055 (2016).

[58] Y. Cohen, Y. Ronen, J.H. Kang, M. Heiblum, D. Feinberg, R. Mélin, and H. Strikman, *Non-local supercurrent of quartets in a three-terminal Josephson junction*, Proc. Natl. Acad. Sci. U. S. A. **115**, 6991 (2018).

[59] A.W. Draelos, M.-T. Wei, A. Seredinski, H. Li, Y. Mehta, K. Watanabe, T. Taniguchi, I.V. Borzenets, F. Amet, and G. Finkelstein, *Supercurrent flow in multiterminal graphene Josephson junctions*, Nano Lett. **19**, 1039 (2019).

[60] K.F. Huang, Y. Ronen, R. Mélin, D. Feinberg, K. Watanabe, T. Taniguchi, and P. Kim, *Quartet supercurrent in a multi-terminal Graphene-based Josephson Junction*, arXiv:2008.03419 (2020).

[61] N. Pankratova, H. Lee, R. Kuzmin, K. Wickramasinghe,1, W. Mayer, J. Yuan, M. Vavilov, J. Shabani and V. Manucharyan, *The multi-terminal Josephson effect*, Phys. Rev. X **10**, 031051 (2020).

[62] G.V. Graziano, J.S. Lee, M. Pendharkar, C. Palmstrom and V.S. Pribiag, *Transport Studies in a Gate-Tunable Three-Terminal Josephson Junction*, arXiv:1905.11730v2 (2020).

[63] E.G. Arnault, T. Larson, A. Seredinski, L. Zhao, H. Li, K. Watanabe, T. Tanniguchi, I. Borzenets, F. Amet and G. Finkelstein, *The multiterminal inverse AC Josephson effect*, arXiv:2012.15253v1 (2020).

[64] S.A. Khan, L. Stampfer, T. Mutas, J.-H. Kang, P. Krogstrup and T.S. Jespersen, *Multiterminal Quantized Conductance in InSb Nanocrosses*, arXiv:2101.02529 (2021).

[65] O. Kürtössy, Z. Scherübl, G. Fülop, I. E. Lukács, T. Kanne, J. Nygard, P. Makk and S. Csonka, *Andreev molecule in parallel InAs nanowires*, arXiv:2103.14083 (2021).

[66] B. van Heck, S. Mi, and A.R. Akhmerov, *Single fermion manipulation via superconducting phase differences in multiterminal Josephson junctions*, Phys. Rev. B **90**, 155450 (2014).

[67] C. Padurariu, T. Jonckheere, J. Rech, R. Mélin, D. Feinberg, T. Martin, and Yu.V. Nazarov, *Closing the proximity gap in a metallic Josephson junction between three superconductors*, Phys. Rev. B **92**, 205409 (2015).

[68] R.-P. Riwar, M. Houzet, J.S. Meyer, and Y.V. Nazarov, *Multiterminal Josephson junctions as topological materials*, Nat. Commun. **7**, 11167 (2016).

[69] E. Eriksson, R.-P. Riwar, M. Houzet, J. S. Meyer, and Y. V. Nazarov, *Topological transconductance quantization in a four-terminal Josephson junction*, Phys. Rev. B **95**, 075417 (2017).

[70] O. Deb, K. Sengupta and D. Sen, *Josephson junctions of multiple superconducting wires*, Phys. Rev. B **97**, 174518 (2018).

[71] V. Fatem, A.R. Akhmerov and L. Bretheau, *Weyl Josephson circuits*, arXiv:2008.13758v1 (2020).

[72] L. Peyruchat, J. Griesmar, J.-D. Pillet and Ç.Ö Girit, *Transconductance quantization in a topological Josephson tunnel junction circuit*, arXiv:2009.03291v1 (2020).

[73] H. Weisbrich, R.L. Klees, G. Rastelli and W. Belzig, *Second Chern Number and Non-Abelian Berry Phase in Topological Superconducting Systems*, PRX Quantum **2**, 010310 (2021).

[74] Y. Chen and Y.V. Nazarov, *Weyl point immersed in a continuous spectrum: an example from superconducting nanostructures*, Phys. Rev. B **104**, 104506 (2021).

[75] Y. Chen and Y.V. Nazarov, *Spin-Weyl quantum unit: theoretical proposal*, Phys. Rev. B **103**, 045410 (2021).

[76] E.V. Repin and Y.V. Nazarov, *Weyl points in the multi-terminal Hybrid Superconductor-Semiconductor Nanowire devices*, arXiv:2010.11494v1 (2020).

[77] B. Douçot, R. Danneau, K. Yang, J.-G. Caputo and R. Mélin, *Berry phase in superconducting multiterminal quantum dots*, Phys. Rev. B **101**, 035411 (2020).

[78] B. Venitucci, D. Feinberg, R. Mélin, B. Douçot, *Nonadiabatic Josephson current pumping by microwave irradiation*, Phys. Rev. B **97**, 195423 (2018).

[79] L.P. Gavensky, G. Usaj, D. Feinberg and C.A. Balseiro, *Berry curvature tomography and realization of topological Haldane model in driven three-terminal Josephson junctions*, Phys. Rev. B **97**, 220505 (2018).

[80] R.L. Klees, G. Rastelli, J.C. Cuevas, and W. Belzig, *Microwave Spectroscopy Reveals the Quantum Geometric Tensor of Topological Josephson Matter*, Phys. Rev. Lett. **124**, 197002 (2020).

[81] H.-Y. Xie, M.G. Vavilov and A. Levchenko, *Topological Andreev bands in three-terminal Josephson junctions*, Phys. Rev. B **96**, 161406 (2017).

[82] H.-Y. Xie, M.G. Vavilov and A. Levchenko, *Weyl nodes in Andreev spectra of multiterminal Josephson junctions: Chern numbers, conductances and supercurrents*, Phys. Rev. B **97**, 035443 (2018).

[83] Yu.V. Nazarov and Y.M. Blanter, *Quantum transport*, Cambridge University Press (2012).

[84] C. Padurariu, T. Jonckheere, J. Rech, T. Martin, and D. Feinberg, *Tunable pseudogaps due to nonlocal coherent transport in voltage-biased three-terminal Josephson junctions*, Phys. Rev. B **95**, 205437 (2017).

[85] J.-D. Pillet, C. Quay, P. Morfin, C. Bena, A. Levy Yeyati, and P. Joyez, *Revealing the electronic structure of a carbon nanotube carrying a supercurrent*, Nature Physics **6**, 965 (2010).

[86] L. Bretheau, J. I-J. Wang, R. Pisoni, K. Watanabe, T. Taniguchi, P. Jarillo-Herrero, *Tunnelling Spectroscopy of Andreev States in Graphene*, Nature Physics **13**, 756 (2017).

[87] J. I-J. Wang, L. Bretheau, D. Rodan-Legrain, R. Pisoni, K. Watanabe, T. Taniguchi, P. Jarillo-Herrero, *Tunneling spectroscopy of graphene nanodevices coupled to large-gap superconductors*, Phys. Rev. B **98**, 121411(R) (2018).

[88] S. Park, W. Lee, S. Jang, Y.-B. Choi, J. Park, W. Jung, K. Watanabe, T. Taniguchi, G. Y. Cho and G.-H. Lee, *Steady Floquet-Andreev States Probed by Tunneling Spectroscopy*, arXiv:2105.00592.

[89] S. B. Kaplan, C. C. Chi, D. N. Langenberg, J. J. Chang, S. Jafarey, and D. J. Scalapino, *Quasiparticle and phonon lifetimes in superconductors*, Phys. Rev. B **14**, 4854 (1976).

[90] R. C. Dynes, V. Narayanamurti, and J. P. Garno, *Direct measurement of quasiparticle-lifetime broadening in a strong-coupled superconductor*, Phys. Rev. Lett. **41**, 1509 (1978).

[91] J.P. Pekola, V. F. Maisi, S. Kafanov, N. Chekurov, A. Kemppinen, Yu. A. Pashkin, O.-P. Saira, M. Möttönen, and J. S. Tsai, *Environment-assisted tunneling as an origin of the Dynes density of states*, Phys. Rev. Lett. **105**, 026803 (2010).

[92] O.-P. Saira, A. Kemppinen, V. F. Maisi, and J. P. Pekola, *Vanishing quasiparticle density in a hybrid Al/Cu/Al single-electron transistor*, Phys. Rev. B **85**, 012504 (2012).

[93] The Supplemental Material presents the technical details of the calculations.

[94] A. Zazunov, V. S. Shumeiko, E. N. Bratus', J. Lantz, and G. Wendin, *Andreev Level Qubit*, Phys. Rev. Lett. **90**, 087003 (2003).

[95] T. Meng, S. Florens and P. Simon, *Self-consistent description of Andreev bound states in Josephson quantum dot devices*, Phys.

Rev. B **79**, 224521 (2009).

[96] D. Averin and H.T. Imam, *Supercurrent noise in quantum point contacts*, Phys. Rev. Lett. **76**, 3814 (1996).

[97] J. C. Cuevas, A. Martín-Rodero, and A. Levy Yeyati, *Hamil-tonian approach to the transport properties of superconducting quantum point contacts*, Phys. Rev. B **54**, 7366 (1996).

[98] C. Caroli, R. Combescot, P. Nozières and D. Saint-James, *Direct calculation of the tunneling current*, Jour. Phys. C: Solid State Phys. **4**, 916 (1971).